AN IMPROVED ACTIVE CONTOUR MODEL FOR MEDICAL IMAGES SEGMENTATION

BY

SHARIF MOHAMMAD SALEH AL-SHARIF

A Thesis Presented to the

DEANSHIP OF GRADUATE STUDIES

KING FAHD UNIVERSITY OF PETROLEUM & MINERALS

DHAHRAN, SAUDI ARABIA

In Partial Fulfillment of the
Requirements for the Degree of

MASTER OF SCIENCE

In

SYSTEMS ENGINEERING

January 2010

KING FAHD UNIVERSITY OF PETROLEUM & MINIRALS

DHAHRAN 31261, SAUDI ARABIA

DEANSHIP OF GRADUATE STUDIES

This thesis, written by SHARIF MOHAMMAD SALEH AL SHARIF under the direction of his thesis advisors and approved by his thesis committee, has been presented to and accepted by the Dean of Graduate Studies, in partial fulfillment of the requirements for the degree of MASTER OF SCIENCE IN SYSTEMS ENGINEERING.

Thesis Committee
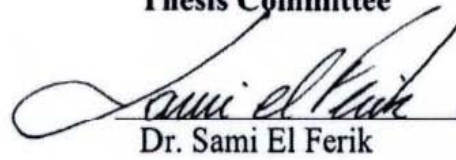
_25/01/2010_

Dr. Sami El Ferik
Thesis Committee Chairman
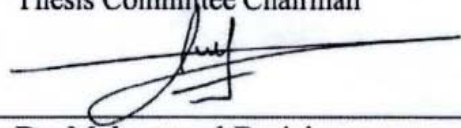
Dr. Mohammad Deriche
Co-Chairman

Dr. Nabil Maalej
Member
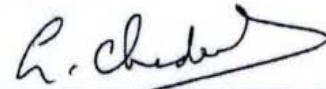
Dr. Lahouari Cheded
Member
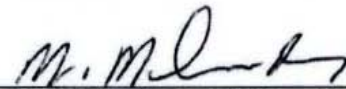
Dr. Mohammad Mohandes
Member

Jan 25,10

Prof. Fouad   Al Sunni
Department Chairman

Dr. Salam Zummo
Dean of Graduate Studies

_6/2/10_

Date

This work is dedicated

to my family, especially to my parents

for their unlimited support along my lifetime.

ACKNOWLEDGMENT

Acknowledgment is due the King Fahd University of Petroleum & Minerals for supporting this research.

I wish to express my deep appreciation to Dr. Mohammed Deriche and Dr. Sami El-Ferik who served as my advisors. I also wish to thank other members of my thesis committee; Dr. Nabil Maalej, Dr. lahouri Cheded and Dr. Mohammed Mohandes.

Also, I would like to acknowledge and express my sincere gratitude to Dr. Omar Al-Turki, Dr. Fouad Al-Sunni, and Dr. Anan Al-Karmi for their continuous support during preparing this work.

Finally, I would like to thank all of my friends and colleagues at KFUPM for helping and supporting me during my life period there.

TABLE OF CONTENTS

CHAPTER ONE

INTRODUCTION   **1**

CHAPTER TWO

REVIEW OF IMAGE SEGMENTATION TECHNIQUES   **5**

CHAPTER THREE

ACTIVE CONTOUR MODELS IN MEDICAL IMAGE SEGMENTATION   **20**

CHAPTER FOUR

HYBRID WAVELET–ACM (WACM) SEGMENTATION TECHNIQUE   **39**

CHAPTER FIVE

EXPERIMENTS AND RESULTS 51

CHAPTER SIX

DISCUSSION AND CONCLUSIONS 87

LIST OF FIGURES

LIST OF TABLES

THESIS ABSTRACT

Name: Sharif Mohammad Saleh Al Sharif.

Thesis Title: An Improved Active Contour Model for Medical Images Segmentation.

Major: Systems Engineering.

Date of Degree: January 2010.

Image Segmentation is an image processing technique which is used to subdivide an image into regions in which each one contains components having similar properties or characteristics. Its goal is to "simplify and/or change the representation of an image into something that is more meaningful and easier to analyze". This approach has many applications. One of its most important applications is the extraction of tumor areas from medical images as a first step in the therapy planning of cancer patients. This objective can be achieved by many image segmentation approaches. One of these successful techniques is the active contour (Snake); its idea is based on a flexible curve (or surface) which is dynamically adapted to required edges or objects in an image. In this work an improvement over a current active contour model is proposed. The new model was tested using real CT images and has given promising results.

MASTER OF SCIENCE DEGREE

King Fahd University for Petroleum & Minerals, Dhahran - Saudi Arabia

JANUARY 2010

ملخص الرسالة

الاسم: شريف محمد صالح الشريف.

عنوان الرسالة: نموذج مطور للمنحنى النشط المستخدم في تجزئة الصور الطبية

التخصص: هندسة النظم.

تاريخ التخرج: يناير 2010.

تعتبر تقنية التجزئة كإحدى تقنيات تحليل الصور , وتستخدم في تقطيع الصورة الى عدة أجزاء بحيث يحتوي كل جزء منها على مكونات تحمل نفس الخصائص أو المميزات. وتهدف هذة العملية الى تبسيط أو تغيير طريقة عرض الصورة بحيث تصبح ذات معنى, كما تعمل هذه الطريقة على تسهيل عملية تحليل الصور.

لهذه التقنية عدة تطبيقات من أهمها عملية تحديد أماكن الأورام في الصور الطبية كمرحلة أولى في التخطيط لعلاج مرضى السرطان . يمكن تطبيق هذة التقنية بعدة أساليب من أنجحها طريقة " المنحنى النشط " أو " الأفعى " والتي يعتمد مبدأ عملها على منحنى (أو سطح) مرن يتكيف ديناميكيا مع شكل حواف الجزء المراد تحديده في الصورة.

خلال هذا البحث تم تطوير نسخة معدلة من تقنية المنحنى النشط (الأفعى), كما تم فحص هذة النسخة بأستخدام صور طبية حقيقية مأخوذة بطريقة التصوير الطبقي المحوري. وقد اعطت النسخة المعدلة نتائج واعدة.

درجة الماجستير في العلوم
جامعة الملك فهد للبترول والمعادن, الظهران – المملكة العربية السعودية
يناير 20 10

CHAPTER ONE

INTRODUCTION

1.1. OVERVIEW OF THE RESEARCH:

The rapid development and proliferation of imaging technologies is revolutionizing medicine. Medical imaging allows scientists and physicians to glean potentially life-saving information by peering noninvasively into the human body. The role of medical imaging has expanded beyond the simple visualization and inspection of anatomic structures. It has become a tool for surgical planning and simulation, intra-operative navigation, radiotherapy planning, and for tracking the progress of disease [1].

Medical image analysis has become one of the most active areas of research these days; many important achievements have been addressed in this field which is vital for physicians who become highly dependent on the image information in order to give an accurate diagnosis of diseases, especially, of tumors, since an early diagnosis of cancer would help very much in treatment. In radiotherapy, medical imaging allows the delivery of a necrotic dose of radiation to a tumor with minimal collateral damage to healthy tissues [1].

The area of medical image processing and analysis covers a wide range of topics, including image acquisition, image formation/reconstruction, image enhancement, image compression and storage, image analysis, and image-based visualization [2]. Medical Image analysis is a promising area of research. It includes many powerful techniques within image analysis, and it has a wide range of applications. One of the well known approaches in medical image analysis is Image Segmentation: its basic is to subdivide the image into regions in which each one contains components having similar properties or characteristics. The goal of segmentation is to simplify and/or change the representation of an image into something that is more meaningful and easier to analyze. In its earlier applications, image segmentation was typically used to locate objects and boundaries (lines, curves, etc.) in images. Now, image segmentation is defined as the process of assigning a label to every pixel in an image such that pixels with the same label share certain visual characteristics [3]. This approach is widely used in extracting tumor areas from medical images as a first step in the therapy planning [39,68] of cancer patients.

Other medical applications for image segmentation, besides locating tumors and other pathologies [69-74], include: measuring tissue volumes [34], computer-guided surgery [76], diagnosis [35,75], localization pathology [36] treatment planning and studying of anatomical structures [37,38]. Beside medical applications of segmentation, segmentation is also used in general Pattern recognition [77], Object detection [78], Machine learning [79], Image or video coding [80,81], Tracking [82-85], and Augmented reality.

1.2. OBJECTIVES OF THE RESEARCH WORK:

The work presented in this thesis focuses on the automatic segmentation of medical images using deformable curves incorporating a priori information. Such priori information is extracted from the region of interest in the original image and used to achieve a faster and a more accurate segmentation. The specific objectives of this research work are as follows:

1. Improving the accuracy of ACM-based medical image segmentation in order to obtain more accurate segmentation for the intended region in the medical image. This will help the physician to be more comfortable with his decision, also, accurate segmentation of the infected region in the medical image of the patient will help the physician to limit the medication only to the infected area, and this will prevent the destruction of the adjacent healthy regions of the patient tissues.

2. Reducing the complexity of the proposedACM-based medical image segmentation algorithm in order to achieve faster segmentation.

3. Evaluating the performance of the proposed algorithm on real medical images. To facilitate the interaction with the algorithm, a GUI is developed, which will also facilitate the task of the medical practitioner.

The entire thesis will be arranged as follows; Chapter two will be a literature review of image segmentation techniques, then, chapter three will focus on active contour models used in medical image segmentation. Chapter four will introduce the Hybrid Wavelet-ACM (WACM) segmentation technique and in chapter six, experiments and results will be discussed. Finally, in chapter seven, conclusions, discussion of the results and future research directions will be presented.

CHAPTER ONE

INTRODUCTION

1.1. OVERVIEW OF THE RESEARCH:

The rapid development and proliferation of imaging technologies is revolutionizing medicine. Medical imaging allows scientists and physicians to glean potentially life-saving information by peering noninvasively into the human body. The role of medical imaging has expanded beyond the simple visualization and inspection of anatomic structures. It has become a tool for surgical planning and simulation, intra-operative navigation, radiotherapy planning, and for tracking the progress of disease [1].

Medical image analysis has become one of the most active areas of research these days; many important achievements have been addressed in this field which is vital for physicians who become highly dependent on the image information in order to give an accurate diagnosis of diseases, especially, of tumors, since an early diagnosis of cancer would help very much in treatment. In radiotherapy, medical imaging allows the delivery of a necrotic dose of radiation to a tumor with minimal collateral damage to healthy tissues [1].

The area of medical image processing and analysis covers a wide range of topics, including image acquisition, image formation/reconstruction, image enhancement, image compression and storage, image analysis, and image-based visualization [2]. Medical Image analysis is a promising area of research. It includes many powerful techniques within image analysis, and it has a wide range of applications. One of the well known approaches in medical image analysis is Image Segmentation: its basic is to subdivide the image into regions in which each one contains components having similar properties or characteristics. The goal of segmentation is to simplify and/or change the representation of an image into something that is more meaningful and easier to analyze. In its earlier applications, image segmentation was typically used to locate objects and boundaries (lines, curves, etc.) in images. Now, image segmentation is defined as the process of assigning a label to every pixel in an image such that pixels with the same label share certain visual characteristics [3]. This approach is widely used in extracting tumor areas from medical images as a first step in the therapy planning [39,68] of cancer patients.

Other medical applications for image segmentation, besides locating tumors and other pathologies [69-74], include: measuring tissue volumes [34], computer-guided surgery [76], diagnosis [35,75], localization pathology [36] treatment planning and studying of anatomical structures [37,38]. Beside medical applications of segmentation, segmentation is also used in general Pattern recognition [77], Object detection [78], Machine learning [79], Image or video coding [80,81], Tracking [82-85], and Augmented reality.

1.2. OBJECTIVES OF THE RESEARCH WORK:

The work presented in this thesis focuses on the automatic segmentation of medical images using deformable curves incorporating a priori information. Such priori information is extracted from the region of interest in the original image and used to achieve a faster and a more accurate segmentation. The specific objectives of this research work are as follows:

1. Improving the accuracy of ACM-based medical image segmentation in order to obtain more accurate segmentation for the intended region in the medical image. This will help the physician to be more comfortable with his decision, also, accurate segmentation of the infected region in the medical image of the patient will help the physician to limit the medication only to the infected area, and this will prevent the destruction of the adjacent healthy regions of the patient tissues.

2. Reducing the complexity of the proposedACM-based medical image segmentation algorithm in order to achieve faster segmentation.

3. Evaluating the performance of the proposed algorithm on real medical images. To facilitate the interaction with the algorithm, a GUI is developed, which will also facilitate the task of the medical practitioner.

The entire thesis will be arranged as follows; Chapter two will be a literature review of image segmentation techniques, then, chapter three will focus on active contour models used in medical image segmentation. Chapter four will introduce the Hybrid Wavelet-ACM (WACM) segmentation technique and in chapter six, experiments and results will be discussed. Finally, in chapter seven, conclusions, discussion of the results and future research directions will be presented.

CHAPTER 2

TECHNIQUES USED IN IMAGE

SEGMENTATION

Many techniques for image segmentation have been proposed in the literature, all of which achieve good accuracy even though they may differ in the way images are analyzed. The following techniques are the most popular approaches. These are clustered into two classes: general purpose segmentation techniques and segmentation techniques used in medical imaging.

2.1.   GENERAL PURPOSE IMAGE SEGMENTATION TECHNIQUES:

Several general-purpose algorithms and techniques have been developed for image segmentation. Since there is no unique solution to the problem, these techniques often have to be combined with domain knowledge in order to effectively solve an image segmentation problem for a given problem domain or application [3].

2.1.1.   Clustering Methods:

This technique [87-89] is based on the "K-means algorithm" [57,86] which was initially proposed in 1956. It is an iterative technique that is used to partition an image into K clusters. The technique is briefly outlined below:

  i.   Choose K cluster centers, either randomly or based on some heuristics.
 ii.   Assign each pixel in the image to the cluster that minimizes the absolute distance between the pixel and the centroid.
iii.   By averaging all of the pixels in the cluster, re-compute the cluster centroid.
 iv.   Repeat steps 2 and 3 until convergence is attained (e.g. no pixels change clusters).

The difference is typically based on pixel color, intensity, texture, and location, or a weighted combination of these factors. K can be selected manually, randomly, or by a

heuristic. Even though the algorithm is guaranteed to converge; it may not return the optimal solution. The quality of the solution depends upon the initial set of clusters and the value of *K*.

In statistics and machine learning, the k-means algorithm is a clustering algorithm used to partition n objects into k clusters, where k < n. It is similar to the expectation-maximization algorithm for mixtures of Gaussians in that they both attempt to find the centers of natural clusters in the data. The model requires that the object attributes correspond to elements of a vector space. The ultimate goal is to minimize the total intra-cluster variance, or, the mean squared error function.

2.1.2.   Methods Based on Histogram:

These techniques [90-93] are very effective when compared to other image segmentation techniques because they typically require only one pass through the pixels. Under this approach, a histogram is computed from all of the pixels in the image, then, the peaks and valleys in the histogram are used to locate the clusters in the image. Color or intensity can be used as the measure. A refinement of this technique is to recursively apply the histogram-seeking method to clusters in the image in order to divide these into smaller clusters. This is repeated with smaller and smaller clusters until no more clusters are formed.

One disadvantage of the histogram-seeking method is that it may be difficult to identify significant peaks and valleys in the image. In this technique of image classification, distance metric and integrated region matching are commonly used

2.1.3.   Methods Based on Edge Detection:

Edge detection is a well-developed field on its own within the image processing. Area, region boundaries and edges are closely related, since there is often a sharp adjustment in intensity at the region boundaries. Edge detection techniques [94-96] have therefore been used as the base of segmentation techniques. The edges identified by edge detection are often disconnected. To segment an object from an image however, one needs closed region boundaries. Discontinuities are bridged if the distance between the two edges is within some predetermined threshold.

2.1.4.   Methods Based on Region Growing:

Region growing [97] is one of the simplest region-based image segmentation methods and can also be classified as pixel-based image segmentation since it involves the selection of an initial seed points. This approach of segmentation examines the neighboring pixels of the initial "seed points" and determines if the pixel should be added

to the seed point or not. The process is iterated in the same way as clustering. The algorithm is briefly described below.

The first approach proposed for region growing was "the seeded region growing method" [3]. The method takes a set of seeds as input from the image. The seeds mark each of the objects to be segmented. The regions are iteratively grown by comparing all unallocated neighboring pixels to the regions. The difference between a pixel's intensity value and the region's mean, δ, is used as a measure of similarity. The pixel with the smallest difference measured this way is allocated to the respective region. This process continues until all pixels are allocated to a region. Seeded region growing requires seeds as additional input. The segmentation results are dependent on the choice of seeds. Noise in the image can cause the seeds to be poorly placed. Unseeded region growing is a modified algorithm that doesn't require explicit seeds. It starts off with a single region A_1 – the pixel chosen here does not significantly influence final segmentation. At each iteration, it considers the neighboring pixels in the same way as seeded region growing. It differs from seeded region growing in that if the minimum δ is less than a predefined threshold T then it is added to the respective region A_j. If not, the pixel is considered significantly different from all current regions A_i and a new region A_{n+1} is created with this pixel.

2.1.5. Methods Based on Level Sets:

Curve propagation is a popular technique in image analysis for object extraction, object tracking, stereo reconstruction, etc. The main idea behind such an approach is to evolve a curve towards the lowest potential of a cost function, where its definition reflects the task to be addressed and imposes certain smoothness constraints. Lagrangian techniques are based on parameterizing the contour according to some sampling strategy and then evolve each element according to image and internal terms. While such a technique can be very efficient, it suffers from various limitations like deciding on the sampling strategy, estimating the internal geometric properties of the curve, changing its topology, addressing problems in higher dimensions, etc.

The level set method was initially proposed to track moving interfaces by [44] and has spread across various imaging domains in the late nineties. It was efficiently used to address the problem of curve/surface/etc. propagation in an implicit manner. The central idea is to represent the evolving contour using a signed function, where its zero level corresponds to the actual contour. Then, according to the motion equation of the contour, one can easily derive a similar flow for the implicit surface that when applied to the zero-level will reflect the propagation of the contour. The level set method has numerous advantages: it is implicit, parameter free, provides a direct way to estimate the geometric properties of the evolving structure, can change the topology and is intrinsic. Furthermore, level sets can be used to define an optimization framework as proposed by

Zhao, Merriman and Osher in 1996 [103]. Therefore, one can conclude that it is a very convenient framework to address numerous applications of computer vision and medical image analysis [58].

2.1.6.   Methods Based on Graph Partitioning:

Graphs can effectively be used for image segmentation. Usually, a pixel or a group of pixels are vertices and edges define the dis-similarity among the neighborhood pixels. Some popular algorithms under this category include Ratio cut [98], random walker, minimum mean cut, minimum spanning tree-based algorithm, normalized cut, etc. The "normalized cuts" method was first proposed by [59]. In this method, the image being segmented is modeled as a weighted, undirected graph. Each pixel is a node in the graph, and an edge is formed between every pair of pixels. The weight of an edge is a measure of the similarity between the pixels. The image is partitioned into disjoint sets (segments) by removing the edges connecting the segments. The optimal partitioning of the graph is the one that minimizes the weights of the edges that were removed (the "cut"). Shi's algorithm seeks to minimize the "normalized cut", which is the ratio of the "cut" to all of the edges in the set.

2.1.7.   Watershed Transformation:

The watershed algorithm [99,100] is an image processing segmentation algorithm that splits an image into areas, based on the topology of the image. The length of the gradients is interpreted as elevation information. During the successive flooding of the gray value relief, watersheds with adjacent catchment basins are constructed. This flooding process is performed on the gradient image, i.e. the basins should emerge along the edges. Normally this will lead to an over-segmentation of the image, especially for noisy image material, e.g. medical CT data. Either the image must be pre-processed or the regions must be merged on the basis of a similarity criterion afterwards [60].

2.1.8.   Model-based segmentation:

The central assumption of such an approach is that structures of interest/organs have a repetitive form of geometry. Therefore, one can use a probabilistic model to explain the variation of the shape of the organ and then use constraints to segment the image. Such a task involves: registration of the training examples to a common pose, probabilistic representation of the variation of the registered samples, and statistical inference between the model and the image. State-of-the-art methods in the literature for knowledge-based segmentation involve active shape and appearance models, active contours and deformable templates and level-set based-methods.

2.1.9.   Multi-Scale Segmentation:

Image segmentations are computed at multiple scales in scale-space and sometimes propagated from coarse to fine scales [61]. Segmentation criteria can be arbitrarily complex and may take into account global as well as local criteria. A common requirement is that each region must be connected in some sense. One of the well known algorithms adopting this segmentation technique is the Connected Coherence Tree Algorithm [101], its goal is to find regions with an adaptive spatial scale and an appropriate intensity-difference scale. This algorithm often forms several sets of coherent neighboring pixels which maximize the probability of being a single image contents. In practice, each set of coherent neighboring pixels corresponds to a coherence class. The fact that each coherence class just contains a single equivalence class ensures the separability of an arbitrary image theoretically. In addition, the resultant coherence classes are represented by tree-based data structures, named connected coherence trees.

2.1.10.   Semi-automatic segmentation:

In this kind of segmentation, the user outlines the region of interest with the mouse clicks and algorithms are applied so that the path that best fits the edge of the image is shown. Techniques like Livewire or Intelligent Scissors are used in this kind of segmentation. The live-wire [102] segmentation technique formulates the problem of creating the boundary of object of interest as a path searching problem in a cost weighted

graph. Its idea is to find the optimal cost paths between a start node and a set of target nodes. If the edges of the object of interest are well defined, these paths will align to the region's outline and form the result of segmentation.

2.1.11. Neural networks-Based segmentation:

Neural Network-based segmentation relies on processing small areas of an image using a neural network or a set of neural networks. After processing, the decision-making mechanism marks the areas of an image accordingly to the category recognized by the neural network. A type of network designed especially for this, is the Kohonen map [62]. In this algorithm, a set of points is initially input to a map consisting of units. Associated with each unit is a weight vector, initially consisting of random values. Units respond more or less to the input vector according to the correlation between the input vector and the unit's weight vector. The unit with the highest response to the input is allowed to learn, as well as some units in the neighborhood. The neighborhood decreases in size during the training period. Learning is done by adjusting the weights of the units by a small amount to resemble the input vector more.

The result of the training is that a pattern of organization emerges in the map. Different units learn to respond to different vectors in the input set, and units closer together will tend to respond to input vectors that resemble each other.

When the training is finished, the set of input vectors is applied to the map once more, marking for each input vector the unit that responds the strongest (is most similar) to that input vector.

2.2. METHODS OF MEDICAL IMAGES SEGMENTATION:

Accuracy is the most important issue in medical images segmentation since the segmented images are used in the therapy planning of patients and this process is an error sensitive process i.e. a small error can cause big problem. Below are techniques are used in medical images segmentation:

2.2.1. Image Segmentation with Deformable Curves:

Medical Images Segmentation is defined as the segmentation of anatomic structures or the partitioning of the original set of image points into subsets corresponding to the structures. It is an essential first stage of most medical image analysis tasks, such as registration, labeling, and motion tracking. These tasks require anatomic structures in the original image to be reduced to a compact, analytic representation of their shapes. Performing this segmentation manually is extremely labor-intensive and time-consuming, and so, many automatic algorithms were proposed to perform this task automatically.

Among the first and primary uses of deformable models in medical image analysis was the application of deformable contour models, such as snakes to segment structures in 2D images [4-14]. Deformable model is set near the object of interest in the image, then, it is allowed to deform towards this object. Users could use the interactive capabilities of these models and manually fine-tune them. Furthermore, once the user is satisfied with the result on an initial image slice, the fitted contour model may then be used as the initial boundary approximation for neighboring slice. These models are then deformed into place and again propagated until all slices have been processed. The resulting sequence of 2D contours can then be connected to form a continuous 3D surface model [6,9,15,16].

The application of deformable models (snakes) to extract regions of interest is not without limitations and in order to get accurate contour, the snake needs to be initialized close to the region of interest, also the internal energy of the contour, which is responsible for its propagation, may affect the performance of the deformable model [1]. Also, the structure of the region of interest must be known in advance.

Many approaches were proposed to improve and further automate the snake segmentation process [1]. Cohen used an internal "inflation" force to expand a snakes model past spurious edges towards the real edges of the structure, making the snake less sensitive to initial conditions [9] (inflation forces were also employed in [17]. Amini used dynamic programming to carry out a more extensive search for global minima[18], while poon et al. [19] minimized the energy of active contour models using simulated annealing

which is known to give global solutions and allows the incorporation of non-differentiable constraints., he also used a discriminant function to incorporate region based image features into the snake [20]. The snake begins as a single closed curve and becomes three closed curves [1].

Image features were also used as a discriminator in snake to lead the deformable contour converge to the exact destination (region of interest) resulting in a more robust energy functional and a much better tolerance to deviation of the initial guess from the true boundaries. Others researchers [21-26] have also integrated region-based information into deformable contour models in an attempt to decrease sensitivity to insignificant edges and initial model placement [1].

2.2.2.   Incorporating Priori Knowledge in Segmentation:

In medical images, the general shape, location and orientation of objects is known beforehand, and this knowledge may be incorporated into the deformable model in the form of initial conditions, data constraints, constraints on the model shape parameters, or into the model fitting procedure. The use of implicit or explicit anatomical knowledge to guide shape recovery is especially important for robust automatic interpretation of medical images. For automatic interpretation, it is essential to have a model that not only describes the size, shape, location and orientation of the target object but also permits expected variations in these characteristics. Automatic interpretation of medical images

can relieve clinicians from the labor-intensive aspects of their work while increasing the accuracy, consistency, and reproducibility of the interpretation [1].

Several researchers casted the deformable model fitting process in a probabilistic framework and included prior knowledge of object shape by incorporating prior probability distributions on the shape variables to be estimated [27-29]. For example, Staib and Duncan used a deformable contour model on 2D echocardiograms and MR images to extract the left ventricle of the heart and the corpus callosum of the brain, respectively [28]. This closed contour model was parameterized using an elliptic Fourier decomposition and a priori shape information which is included as a spatial probability expressed through the likelihood of each model parameter. The model parameter probability distributions are derived from a set of example object boundaries and serve to bias the contour model towards expected or more likely shapes [1].

2.2.3.   Volume Image Segmentation with Deformable Surfaces:

This process is a slice-by-slice segmentation   of 3D image volumes, either manually or by applying 2D contour models. It is a laborious process and requires a post-processing step to connect the sequence of 2D contours into a continuous surface. Moreover, the resulting surface reconstruction can contain inconsistencies or show rings or bands. The use of a true 3D deformable surface model on the other hand, can result in a faster, more robust segmentation technique which ensures a globally smooth and coherent surface between image slices. Deformable surface models in 3D

were first used in computer vision in 1988 [30], since then, many researchers have used this technique and improved upon it using some post processing tools.

CHAPTER THREE

ACTIVE CONTOUR MODELS

IN MEDICAL IMAGE SEGMENTATION

3.1. OVERVIEW:

The most popular approaches brought to maturation during 1980s and 1990s in terms of both methodology development and application were boundary finding strategies based on deformable models (snakes) [2]. A snake, which is a fundamental approach in image analysis, was first introduced in 1987 by Kass et al. [4]. Since then, it became an area of successful research for image segmentation. The snake is a deformable continuous

curve; whose shape is controlled by forces applied upon it. Its objective is to divide an image into a number of strongly correlated objects. This objective is a difficult task because of the big variability of object shapes and different image quality [32]. Many people have proposed various definitions of snakes in the literature. All of these definitions lead to the same meaning but with different words. The following are some of these: (1) It is the grouping of parts in an image into units that are homogeneous with respect to one or more features, another definition is given as (2) The maximization of the mutual information between the region labels and the image pixel intensities subject to a constraint on the total length of the region boundaries, a third definition is (3) The partitioning of an image into a finite number of semantically important regions. One more definition is given as (4) An energy minimizing spline that detects specified features within an image. It is a flexible curve (or surface) which can be dynamically adapted to required edges or objects in the image. It can be used for automatic image segmentation. This approach is found in the literature under different names such as snakes, active contours, surfaces or balloons. The active contour consists of a set of control points connected by straight lines. It is defined by the number of control points as well as their sequence. Shaping the image by fitting active contours is an interactive process in which an initial contour needs to be suggested by the user (should be as close as possible to the intended shape). The contour is attracted to the features in the image extracted by internal energy creating an attracter image.

Active contour "Snakes" techniques have been used in many applications, one of its most important uses is the tumor areas extraction from medical images which is used as a first step in the therapy planning of cancer patients. Other medical applications are measurement of tissue volumes, computer-guided surgery, diagnosis, treatment planning and study of anatomical structure. Beside medical applications of segmentation, snake has also been used in pattern recognition, object detection, machine learning, image or video coding, tracking, and augmented reality.

3.2. MEDICAL IMAGE SEGMENTATION USING ACTIVE CONTOUR MODEL:

The main idea here is to isolate and extract individual components from a medical image. This is an important part of medical imaging; once a shape is found, physicians can measure various quantities, such as size of tumors, thickness of heart walls … etc. Tracing the boundary of these shapes by hand is time-consuming. Instead, the goal is an automatic segmentation technique which finds the desired regions without human interaction. Suppose that we are given a medical image; say a digital subtraction angiogram - DSA (see figure.3.1) [63].

Figure.3.1. DSA Image of an Artery

Suppose that we want to extract the important features within this image; in this case, the outline of the artery. One idea is to look for places where there is a big jump in intensity between neighboring pixels. However, it is hard to pick a good value for the jump; too small and you get extra boundaries; too large and you miss the whole target. Another problem is that we can get fooled by large spikes of noise. A different approach comes from initializing a small circle inside the region of interest, and allowing it to grow outwards until it reaches the desired boundary (see figure.3.2). This is a typical example of an active contour that starts with an initial contour then propagates toward the edges of the image under the control of the contour and other image forces.

Figure.3.2. Segmentation of a DSA Image

3.3.   DEFORMABLE MODELS:

Active contour Models (ACM) or Snakes were first introduced by Kass et al. [4] in 1987, since then, ACM became an active area of research. The approach is based on a

flexible curve (or surface) which is dynamically adapted to required edges or objects in the image. There are two basic types of deformable models; *parametric deformable models* [4,6,18,31] and *geometric deformable models* [40-43].

3.3.1.   Parametric Deformable Models:

Parametric deformable models, proposed by Kass et al. in 1987 [4], represent curves and surfaces that are explicit in their parametric forms during deformation. This representation allows direct interaction with the model and can lead to a compact representation for fast real-time implementation. Adaptation of the model topology, however, such as splitting or merging parts during the deformation, can be difficult using parametric models. There are two types of formulations for parametric deformable models; the *energy minimizing formulation* which searches for parametric curve that minimizes weighted sum of the internal and external energies, where the internal energy specifies the tension or the smoothness of the contour, while the external energy is defined in the image domain and usually has a minimal value at the point where there is a high intensity gradient in the image, i.e. at an object edge. In this technique, the total energy minimization occurs when the internal and the external energies are equal [63]. The second formulation for parametric deformable models is the *dynamic force formulation* which is used in cases where it is more comfortable to form a deformable model straight from the dynamic problem with the help of force formulation. Despite the fact that these two formulations lead to similar results, the first formulation has the

simplicity advantage since its solution satisfies a minimum principle while the second formulation is flexible to allow the use of more general types of external forces, even those which are not potential ones such as the forces which cannot be described by a negative gradient of potential energy function [63].

3.3.1.1.   Energy minimizing formulation:

The basic concept of energy minimization in deformable contours is to find a parameterized curve that minimizes the weighted sum of *internal energy* and *potential energy* [65]. The internal energy specifies the tension or the smoothness of the contour, it depends on the intrinsic properties of the curve and it is a sum of two types of energy; *elastic energy* and *bending energy*. The elastic energy treats the curve as a rubber band; it discourages stretching of the curve by introducing tension (see figure 3.3). It is mathematically described as the sum of the squared rate of change of the position of each point in the contour (see the first term in eq.3.2). A weight $\alpha(s)$ allows us to control the elastic energy along different parts of the contour and is always considered to be constant α for many applications. The bending energy forces the contour to behave as a thin metal disc (see figure 3.4), it discourages bending of the curve, and as a result, the contour is forced to slow down when it reaches the sharp edges and precisely takes its shape. Bending energy is formulated as the sum of the squared curvature of the contour.
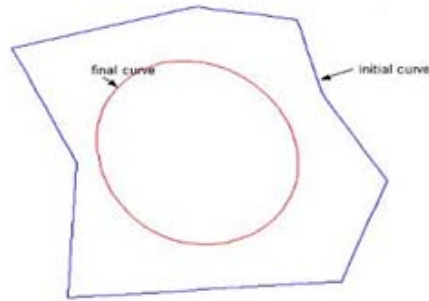
Figure3.3. Elastic Energy Effect on the Curve

The term β(s) is multiplied by the bending energy (in the second term of eq.3.2) in order to control this energy along the contour, and is always considered to be constant for many application.
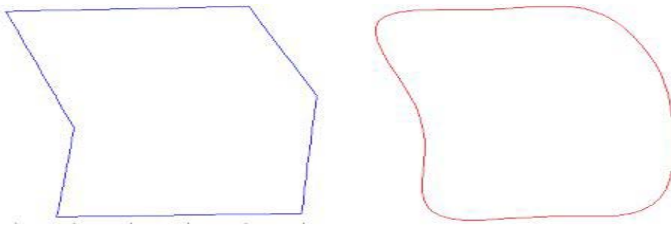
Figure3.4. Effect of Bending Energy on the Curve (Left) Initial Curve (High Bending Energy) (Right) Final Curve Deformed by Bending Force (Low Bending Energy)

The potential energy is defined over the image domain and typically possesses local minima at the image intensity edges occurring at object boundaries. Minimizing the total energy yields *internal forces* and *potential forces*. Internal forces hold the curve together (elastic forces) and keep it from bending too much (bending forces). External

forces attract the curve toward the desired object boundaries (see figure 3.5). To find the object boundary, parametric curves are initialized within the image domain, and are forced to move toward the potential energy minima (or maximum gradient of the image which is near its edges) under the influence of both these forces.
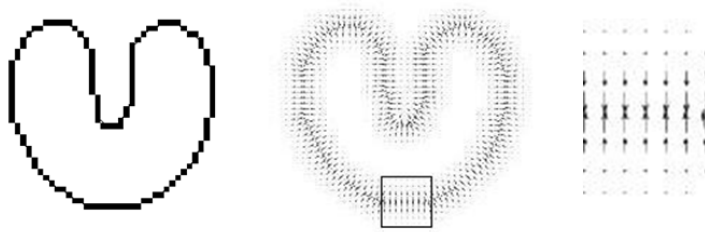
Figure3.5 Potential Force, (Left) Original Image, (Middle) External Forces, (Right) Zoomed in External Forces

Mathematically, a deformable contour is a curve $\mathbf{X}(s) = (x(s),y(s))$, which moves through the spatial domain of an image to minimize the following energy functional [65]:

$$\varepsilon(\mathbf{X}) = E_{snake} = \int_0^1 E_{snake}\left(\boldsymbol{X}(s)\right)ds = \int_0^1 \left[E_{int}\left(\boldsymbol{X}(s)\right) + E_{ext}\left(\boldsymbol{X}(s)\right)\right] ds$$

where

$$\varepsilon(\mathbf{X}) = S(\mathbf{X}) + \mathcal{P}(\boldsymbol{X}) \qquad\qquad 3.1$$

The first term is the internal energy functional and is defined to by:

$$S(\mathbf{X}) = \frac{1}{2} \int_s \left[\alpha(s) \left| \frac{\partial \mathbf{X}}{\partial s} \right|^2 + \beta(s) \left| \frac{\partial^2 \mathbf{X}}{\partial s^2} \right|^2 \right] ds \qquad 3.2$$

The internal energy is composed of two types of energy; the first one is the elastic energy which is the first term in eq.3.2, and the bending energy which is the second term in eq.3.2. The first-order derivative discourages stretching and makes the model behave like an elastic string (i.e. smoothes the contour). The second-order derivative discourages bending and makes the contour behave like a thin metal disc (i.e. slows down the contour when it gets near the edges of the region of interest in order to force it to take the shape of the edges) as shown in figure 3.4. The weighting parameters $\alpha(s)$ and $\beta(s)$ can be used to control the strength of the model's tension and rigidity, respectively. In practice, $\alpha(s)$ and $\beta(s)$ are often chosen to be constants [65].

The second term is the external or potential energy functional is calculated by integrating a potential energy function P(x,y) *along the contour* $\mathbf{X}$(s) [65].

$$\mathcal{P}(\boldsymbol{X}) = \int_0^1 P\big(\boldsymbol{X}(s)\big) \, ds \qquad 3.3$$

The potential energy function P(x,y) is derived from the image data. It takes smaller values at object boundaries as well as other features of interest. Given a gray-level image I(x,y) viewed as a function of continuous spatial variables, (x,y), [65] a typical

potential energy function is designed to make a deformable contour converge toward step edges (see eq.3.4):

$$P(x, y) = -\omega_e |\nabla[G_\sigma(x, y) * I(x, y)]|^2 \qquad \text{3.4}$$

Where ω_e is a positive weighting parameter, $G_\sigma(x, y)$ is a two-dimensional Gaussian function with standard deviation σ (see equn.3.5), $\nabla(.)$ is the gradient operator, and * is a 2D image convolution operator. Note that the integration in equn.3.3 is only over P(x,y) corresponding to the contour $\mathbf{X}$(s).

For the edge potential energy, increasing σ can broaden its attraction range since the use of a large σ decreases the attenuation of low frequencies, resulting in decreased blurring in the attracter image [66]. However, using a larger value for σ can also cause a shift in the location of the boundary which leads to a less accurate result [65].

$$G_\sigma(x, y) = K.e^{\frac{-((x-x_0)^2 + (y-y_0)^2)}{2\sigma^2}} \qquad \text{3.5}$$

Regardless of the selection of the exact potential energy function, the procedure for minimizing the energy functional is the same [65]. The problem of finding a curve $\mathbf{X}(s)$ that minimizes the energy functional $\boldsymbol{\varepsilon}$ is known as a variational problem. The curve that minimizes $\boldsymbol{\varepsilon}$ must satisfy the following Euler-Lagrange equation:

$$\frac{\partial}{\partial s}\left(\alpha \frac{\partial X}{\partial s}\right) - \frac{\partial^2}{\partial s^2}\left(\beta \frac{\partial^2 X}{\partial s^2}\right) - \nabla P(X) = 0 \qquad 3.4$$

To gain some insight about the physical behavior of deformable contours, we can view eq.3.6 as a force balance equation.

$$F_{int}(X) + F_{pot}(X) = 0 \qquad 3.5$$

where the internal force is given by:

$$F_{int}(X) = \frac{\partial}{\partial s}\left(\alpha \frac{\partial X}{\partial s}\right) - \frac{\partial^2}{\partial s^2}\left(\beta \frac{\partial^2 X}{\partial s^2}\right) \qquad 3.6$$

and the potential force is given by

$$F_{pot}(X) = -\nabla P \qquad 3.7$$

The internal force F_{int} discourages stretching and bending while the potential force F_{pot} pulls the contour toward the desired object boundaries. Here, we define the forces derived from the potential energy function P(x,y), given in eq.3.4 , as *Gaussian potential forces*.

To find a solution to eq.3.6, the deformable contour is made dynamic by treating $X(s)$ as a function of time t as well as $\mathbf{s}$ — i.e. $X(s,t)$. The partial derivative of X with respect to t is then set equal to the left-hand side of eq.3.6 as follows:

$$\gamma \frac{\partial X}{\partial t} = \frac{\partial}{\partial s}\left(\alpha \frac{\partial X}{\partial s}\right) - \frac{\partial^2}{\partial s^2}\left(\beta \frac{\partial^2 X}{\partial s^2}\right) - \nabla P \qquad\qquad 3.\,8$$

The coefficient γ is introduced to make the units on the left side consistent with the right side. When the solution $X(s,t)$ stabilizes, the left side vanishes and we achieve a solution of eq.3.6. We note that this approach of making the time derivative term vanish is equivalent to applying a gradient descent algorithm to find the local minimum of eq.3.1. Thus, the minimization is solved by placing an initial contour on the image domain and allowing it to deform according to eq.3.10.

3.3.1.2.   Dynamic forces formulation:

In the previous section, the deformable model was modeled as a static problem. However, it is sometimes more convenient to formulate the deformable model directly from a dynamic problem using a force formulation. Such a formulation permits the use of more general types of external forces which are often expressed as the superposition of several different forces [65]:

$$F_{ext}(X) = F_1(X) + F_2(X) + \cdots + F_N(X) \qquad\qquad 3.\,11$$

where N is the total number of external forces. This superposition formulation allows the external forces to be broken down into more manageable terms [65].

3.3.2. Geometric Deformable Models:

Geometric deformable models were independently proposed by Caselles et al. [40] and Malladi et al.[41]. They can handle topological changes naturally. These models are based on two techniques; the first one is the theory of curve evolution [65], which is a famous theorem in differential geometry that had been proved less than ten years ago. This theory says that **"any simple closed curve moving under its curvature collapses nicely to a circle and then disappears. That is, no matter how wildly twisting a curve is, as long as it is simple, it will "relax" to a circle and then disappear".** The purpose of curve evolution theory is to study the deformation of curves using only geometric measures such as the unit normal and curvature as opposed to the quantities that depend on parameters such as the derivatives of an arbitrary parameterized curve. The second technique which gives the basics for geometric deformable models is the level set method [44], this technique represents curves and surfaces implicitly as a level set of a higher-dimensional scalar function, the models parameterizations are computed only after complete deformation, thereby allowing topology to be adaptively and easily accommodated.

3.3.2.1.   Level set method:

The level set method is used to account for automatic topology adaptation. It offers the basis for a numerical scheme that is used by geometric deformable models. The level set method for evolving curves was initially proposed by to Osher and Sethian [44,46,48].

In the level set method, the curve is represented implicitly as a level set of a two dimensional scalar function referred to as the "level set function". This function is usually defined in the same domain as the image. The level set is defined as the set of points that have the same function value. The only purpose of the level set function is to provide an implicit representation of the evolving curve. Instead of tracking a curve through time, the level set method evolves the curve by updating the level set function at fixed coordinates through time. This perspective is similar to that of an Eulerian formulation of motion as opposed to a Lagrangian formulation which is analogous to the parametric deformable model. A useful property of this approach is that the level set function remains a valid function while the embedded curve can change its topology [65].

Suppose that you are given a curve separating one region from another, and a force F that tells you how to move each point of the curve. In the figure.3.6 [64] below, a black curve separates two regions, and at each point of the black curve the force F is given. This force can depend on many physical effects.
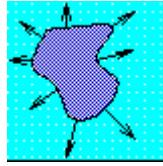
Figure3.6 Example of a Curve Separating Two Regions

Most numerical techniques depend on markers, which tracks the motion of the boundary by breaking it up into buoys that are connected by pieces of rope. The idea is to move each buoy under the force F depending on the connecting ropes to keep things straight. The hope is that more buoys will make the answer more accurate, but this is not always the case, since in many cases the buoys try to cross over themselves, or the curve tries to break into two. In these cases, it is very hard to keep the connecting ropes organized [64].

Instead of following the curve itself, the level set technique introduced by Osher and Sethian [44] takes the original curve (see figure 3.7-a) and builds it into a surface. That cone-shaped surface, which is shown figure 3.7-b, has an excellent property; it intersects the xy plane *exactly* where the curve sits. The surface in figure 3.7-b is called the level set function; because it accepts any point in the plane as input and returns its height as output. The initial contour (figure 3.7-a) is called the zero level set, because it is the collection of all points that are at height zero [64].
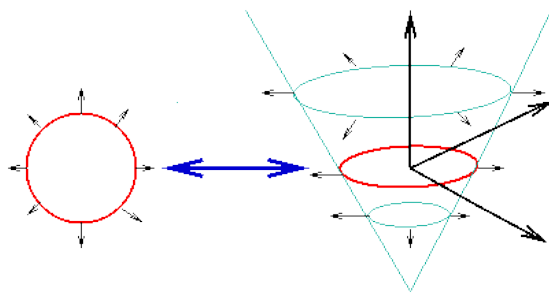
**Figure3.7. Level Set Function (Left) The Original Curve (xy Plane),
(Right) The Level Set Function (Curve is in Intersection with Surface and xy Plane)**

The idea of the level set is that; the surface (figure 3.7-b) moves instead of moving the curve (figure 3.7-a). By this, we can get rid of all sorts of weird things that may happen when the curve deforms. In other words, the level set function expands, rises, falls, and does all the work [64]. The technique of level set is called "Initial Value Formulation" since its solution starts at a given position and evolves in time (figure 3.8).
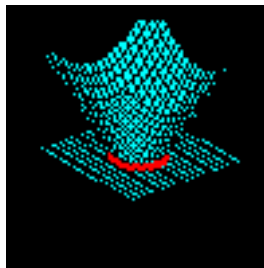
Figure3.8 Evolution of Level Set

The advantage of the level set approach over the traditional curve evolution is that the level set approach allows the evolving curve to change topology, break, and

merge, which means that the evolving curve can extract the boundaries of particularly complicated contours. In addition, this technique works in three dimensions with almost no change, so three dimensional surfaces can be extracted as well [64].
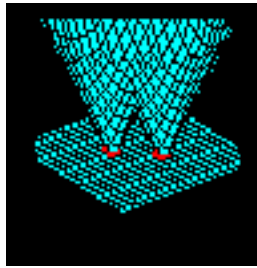
Figure3.9 Two Initial Curves Joins Together as they Grow

3.3.2.2.   Moving the Contour:

Active contour is used to determine the real boundary of an object of interest in an image. To do this, an initial guess of the boundary of an object of interest is done by the user. Then, the contour starts its evolution until it reaches the actual boundary of the object of interest. Active contour is a collection of points in the plane:

$$V = \{v_1, \dots, v_n\}$$

$$v_i = (x_i, y_i), i = 1, \dots, n \qquad\qquad 3.12$$

The points in the contour iteratively approach the boundary of an object through the solution of an energy minimization problem. For each point in the neighborhood of v_i an energy term is computed:

$$E_i = \alpha E_{int}(v_i) + \beta E_{ext}(v_i) \qquad\qquad 3.13$$

Where E_i, E_{int} and E_{ext} are matrices. The value at the center of each matrix corresponds to the contour energy at point v_i. Other values in the matrices correspond spatially to the energy at each point in the neighborhood of v_i.

Each point, v_i, is moved to the point, v_i', corresponding to the location of the minimum value in E_i (see figure 3.10) [104].
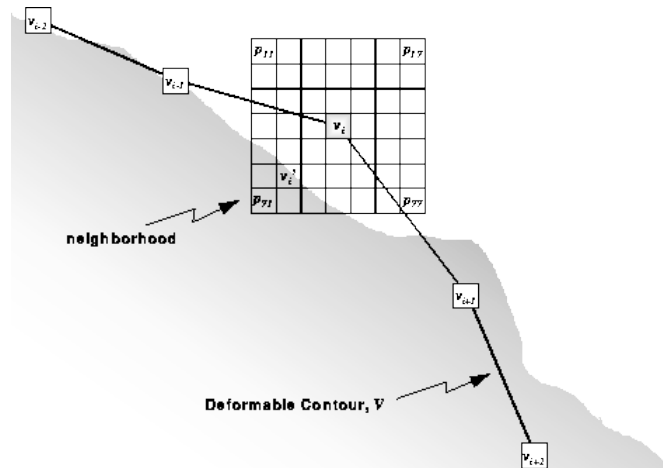
Figure3.10 Moving the Contour Iteratively Under the influence of Energy

3.3.2.3. Formulation of the Speed Function:

In image segmentation, active contours are defined as dynamic curves that move toward object boundaries [49]. To accomplish this objective, an external energy is defined. This energy moves the zero level contour (see section 3.3.2.1) toward object boundaries. Suppose that I is an image, the stopping function g is formulated as follows:

$$g(\nabla I) = \frac{1}{1+|\nabla(G_\sigma * I)|^2} \qquad \qquad 3.\,14$$

where G_σ is a Gaussian kernel with a standard deviation σ. It is used to reduce the noise in the image. The curve evolution is connected with the image data using the stopping function g. This technique works well for objects having good contrast. On the other hand, when the object boundary is blurred or has gaps, the geometric deformable contour may fail to catch the boundary because the stopping function slows down the curve near the boundary instead of completely stopping it. If the contour passes the boundary, it will not be pulled back to recover the correct boundary. To remedy this problem, Caselles et al. [42] used the stopping function in eq.3.15, where $\beta > 0$ controls the convergence speed of the stopping function. The geometric active contour model is expressed as a diffusion equation by using the level set technique with the original curve **X**(s,t).

$$g(\nabla I) = \frac{1}{1+\beta\,|\nabla(G_\sigma * I)|^2} \qquad \qquad 3.15$$

CHAPTER FOUR

HYBRID WAVELETS-ACM

SEGMENTATION TECHNIQUE

4.1.   BASIC DEFINITIONS:

Since the last few years, the work in the segmentation area has been concentrated on geometric active contours technique i.e. the active contours which are implemented via level set methods. The goal of this work is to address a wide range of image segmentation problems in image processing and computer vision [49]. Active contours are

mathematically defined as a set of the coordinates of control points on the contour [33].They are parametrically defined as follows:

$$v(s) = (x(s), y(s))$$ 4.1

where x(s), and y(s) are x,y coordinates over the contour, and s is the normalized index of the control points. The active contour is described by an energy function which is composed of two types of energy components. The first component is the internal energy which makes the curve elastic (elastic energy $E_{elastic}$) and limits its sharp deflections (bending Energy $E_{bending}$). The second component is the external energy which pushes the curve towards the object borders [33]. The internal energy can be described as follows:

$$E_{int} = E_{elastic} + E_{bending} = \alpha(s)\left|\frac{\partial v}{\partial s}\right|^2 + \beta(s)\left|\frac{\partial^2 v}{\partial s^2}\right|^2$$ 4. 2

where α is an adjustable constant that specifies continuity, and β is an adjustable constant that specifies contour curving [33]. Both variables are usually chosen as constants which are used to control the internal energy over the whole contour (see section 3.3.1).

The elastic energy is defined as the sum of the squared distances between each two adjacent points in the active contour. It is mathematically described as follows:

$$E_{elastic} = \int_s \alpha(v(s) - v(s-1))^2 ds \qquad\qquad 4.3$$

The bending energy is defined as the sum of the squared curvatures for all points along the contour. Mathematically, it is the described as the elastic energy derivate.

$$E_{bending} = \int_s \beta(v(s-1) - 2v(s) - v(s+1))^2 ds \qquad\qquad 4.4$$

The external energy is extracted from the image to be segmented. It depends on the gradient of this image. It is usually formulated as follows:

$$E_{external} = \frac{1.}{1+|G_\sigma(x,y)*I(x,y)|^2} \qquad\qquad 4.5$$

where I(x,y) is the image to be segmented and G_σ is a Gausssian kernel used to smooth the image in order to facilitate the segmentation process. The energy function which is needed to be minimized in order to achieve the segmentation process is expressed in eqn.(4.6).

$$E_{snake} = \int_0^1 E_{snake}(v(s))ds = \int_0^1 E_{int}(v(s)) + E_{ext}(v(s)) \, ds \qquad\qquad 4.6$$

4.2.   ANALYSIS USING INTENSITY PRIORS:

In 2008, H. Zhang *et.al.* [55] proposed a new method for enhancing the classical geometric active contours (GAC) model by incorporating 'prior' information into the scheme. The modified model was applied to biomedical imagery, specifically serial ultrathin electron microscopy sections. The technique was used to apply prior analysis on a training set of data and provide geometric information about the target object during the process of curve evolution. Experiments on synthetic and real images were performed using the new technique. The analysis of results showed that the approach works better than the previous methods. The proposed technique was implemented in semi-automated fashion and gave noticeable improvements over manual schemes.

4.2.1   Intensity Priors:

Sometimes, curve evolution becomes sensitive and unstable so that the final result in some cases will be inaccurate or missing the real boundary [55]. To remedy this problem, a number of points on the boundary of the region of interest (ROI) in the image are manually selected to generate a training set. This set will represent the region of interest but it needs to be further analyzed to discard some outliers since the selection is effectively subjective. " Suppose that the image under analysis is in the gray scale, the samples are gray pixels and their intensities are fairly concentrated so that we assume the samples follow a 'univariate' normal distribution and the variance is known empirically"

[55]. As a result of a statistical analysis for the set of points, an intensity interval is obtained by the following procedure:

1. The mean u and variance σ^2 of the parameters is calculated.

2. The range of intensity values around the boundary of ROI is estimated by using a confidence interval at a given confidence level (c). See equn.4.7 where z^* is the critical value of (1-c/2) where c in the confidence level [0,1].

$$\left(\overline{x} - \frac{\sigma}{\sqrt{n}} z^*, \ \overline{x} + \frac{\sigma}{\sqrt{n}} z^*\right)$$ 4. 7

3. If there is any intensity value that is out of the calculated range, it will be discarded.

4. Because the samples come from the same statistical distribution, interval analysis is used (eqn.4.8) to further to improve the intensity interval after discarding the 'outliers'. See equn.4.8 where s_i, i=1 ... n, are the samples intensities, and m is the mean of the intensities follows the t(n-1) student distribution.

$$S = \sqrt{\frac{1}{n-1} \Sigma_{i=1}^n (s_i - m)^2}$$ 4. 8

5. For a degree of belief α, a confidence interval is created according to t-distribution. The degree of belief that the sample lies in the confidence interval is (1-α) %, so, the confidence interval will be as follows [55].

$$\left[m - \frac{s}{\sqrt{n}} t_{\frac{\alpha}{2}} , m + \frac{s}{\sqrt{n}} t_{\frac{\alpha}{2}}\right] \qquad\qquad 4.9$$

where $t_{\frac{\alpha}{2}}$ is the corresponding value of the degree of belief α in the t-distribution.

4.2.2   Geometric Priors:

Because the prior analysis is relative to a region of interest in the image, noise around the region of interest may still affect the curve evolution. This effect leads the contour to converge to false edge. By providing the contour with some geometric information, curve evolution can 'traverse' regions of non-interest in order to successfully arrive to the boundary of the object of interest [55]. In the training set, every point is selected on the object boundary before starting prior analysis (see the previous section). Also, a number of points can be chosen around the ROI in order to form a polygon by these points. This polygon will enclose the target object in order to facilitate the curve evolution and traverse any noise in the area. In some applications, a circle is needed to be formed around the ROI instead of the polygon, to do this, a 'center' point of the region of interest, (x_0, y_0), and a 'radius' of the circle, R, are needed to be specified. By this, the formed circular shape covers the whole region of interest (see figure 4.1).
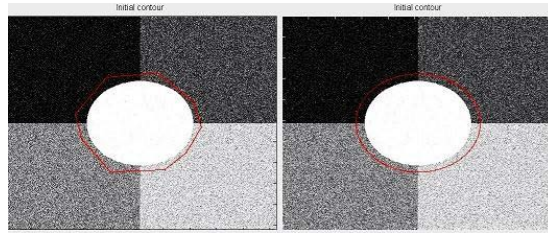
Figure.4.1. Initial Contour: (Left) Polygon, (Right) Circle

4.2.3   Incorporating Priors into GAC Models:

In GAC approach, the stopping function g(.) plays a critical role since it controls the arrival time of the active contour at the boundary of ROI during the iterative approximation procedure. Note that the value of g(.) at image boundaries is closer to zero, while it is close to 1 in the homogeneous regions in the image.

$$g(|\nabla I|) = \frac{1}{1+|\nabla(G_\sigma * I)|^2}$$

4. 10

In order to affect the process of curve evolution, we can rebuild the stopping function according to the collected prior information. Our technique is to modify the stopping function using this prior information in order to make its value closer to zero while the contour is approaching to the boundary of ROI. Since the image gradient near its boundary is high, the following indicator function λ(*x*) is used [55]:

$$\lambda(x) = \begin{cases} 1 & x \epsilon \Theta \\ 0 & otherwise \end{cases} \qquad\qquad 4.\ 11$$

where x is the image data (such as the intensity of a pixel) and Θ stands for some prior information such as the intensity interval. Then, the indicator function is smoothed with a Gaussian kernel and subsequently multiplied with the smoothed image. Based on the above, we proposed to change the stopping function g (in eqn.4.10) in the following manner:

$$g(|\nabla I|) = \frac{1}{1+\beta(x)\bullet|\nabla(G_\sigma * I)|^2} \ , \beta(x) = G_\sigma * \lambda(x) \qquad\qquad 4.\ 12$$

In eqn.4.12, β is no longer a simple weight but is a matrix formed by the convolution of the Gaussian G_σ with the indicator function $\lambda(x)$, and $\bullet$ indicates point-to-point array multiplication [55].

4.3.   MODIFYING THE STOPPING FUNCTION:

The speed function can be improved more to achieve faster convergence to the region of interest in the image, below there are some suggested stopping function that we investigated.

$$g(|\nabla I|) = \frac{1}{1+e^{\beta(x)\bullet M}} \ , M = |\nabla(G_\sigma * I)|^2 \qquad\qquad 4.\ 13$$

After expanding the exponential term in equn.4.13 using Taylor series it becomes as follows:

$$g(\nabla I) = \frac{1}{2 + \beta(x) \cdot M + \frac{\beta(x)^2 \cdot M^2}{2!} + \frac{\beta(x)^3 \cdot M^3}{3!} + \frac{\beta(x)^4 \cdot M^4}{4!}} \qquad 4.\ 14$$

In the stopping function of eq.4.13, the exponential function is integrated with the stopping parameters in the denominator of eq.4.12. The aim of this integration is to increase the speed of convergence of the stopping function in eq.4.12, since it is known from mathematics that the exponential function has the fastest increase over other functions, and so, if this function is added in the denominator of the stopping function, the stopping function will decrease faster. Using this technique, it is expected to increase the speed of convergence of the active contour by a noticeable percentage. In eq.4.14, the exponential term in eq.4.13 is expanded using Taylor series up to the fourth order. This modification in the stopping function is expected to increase the speed of convergence of the stopping function by decreasing the computation time. The expansion of the exponential function is stopped after the fourth order since there will be no improvement in the speed of the contour after this order. This result was obtained by trial. The results of implementing eqs.4.12, 4.13, and 4.14 and their effects over the speed of the active contour will be presented and discussed in the following chapters.

4.4. IMPROVING THE MODEL USING THE WAVELET TRANAFORM:

Wavelets are mathematical functions that cut up data into different frequency components, and then study each component with resolution matching its scale [67]. One of the important techniques used in wavelet is signal decomposition which is a sampling technique used to decrease the complexity of the signal in order to facilitate its study. One of the important Matlab commands which are used to perform this task over two dimensional data is "dwt2". Using this command to decompose an image results in a sampled image identical to the original one but with its size ¼ of the original one (figure.4.2).

Figure.4.2 Processing an Image Using Wavelet
(Left) Original Image, (Right) Decomposed Image

By using this technique on an image before starting its segmentation and then start the segmentation process of the decomposed image, the speed of the active contour is expected to be noticeably increased. The final contour from this process can be used as

an initial contour to segment the original image. This procedure is expected to decrease the time required for segmenting large images such as medical images.

The procedure in which the developed model follows is described below:

1.   At the beginning, an image to be segmented is loaded and smoothed.

2.   The loaded image I is decomposed using wavelet transform. The output of this step is a decomposed image I_d.

3.   A Set of points are chosen around the region of interest in the image I_d.

4.   The confidence interval of intensities of the selected points is computed.

5.   The β matrix is formed depending on the confidence interval.

6.   The gradient of the image I_d is computed and the stopping function is formed depending on β matrix.

7.   An Initial contour is chosen and evolution is started. This contour is run for a fixed number of iterations.

8.   Steps 3 – 6 are repeated but this time for the original image I.

9.   The final contour of step 7 is loaded as an initial contour for segmenting the original image, evolution resumed.

10.   When the active contour reaches the ROI, in the real image, it stops there and the final result of segmentation is displayed.

The data flow diagram which describes the listed procedure of the Wavelet Active Contour Model (WACM) algorithm described above is shown in figure 4.3:
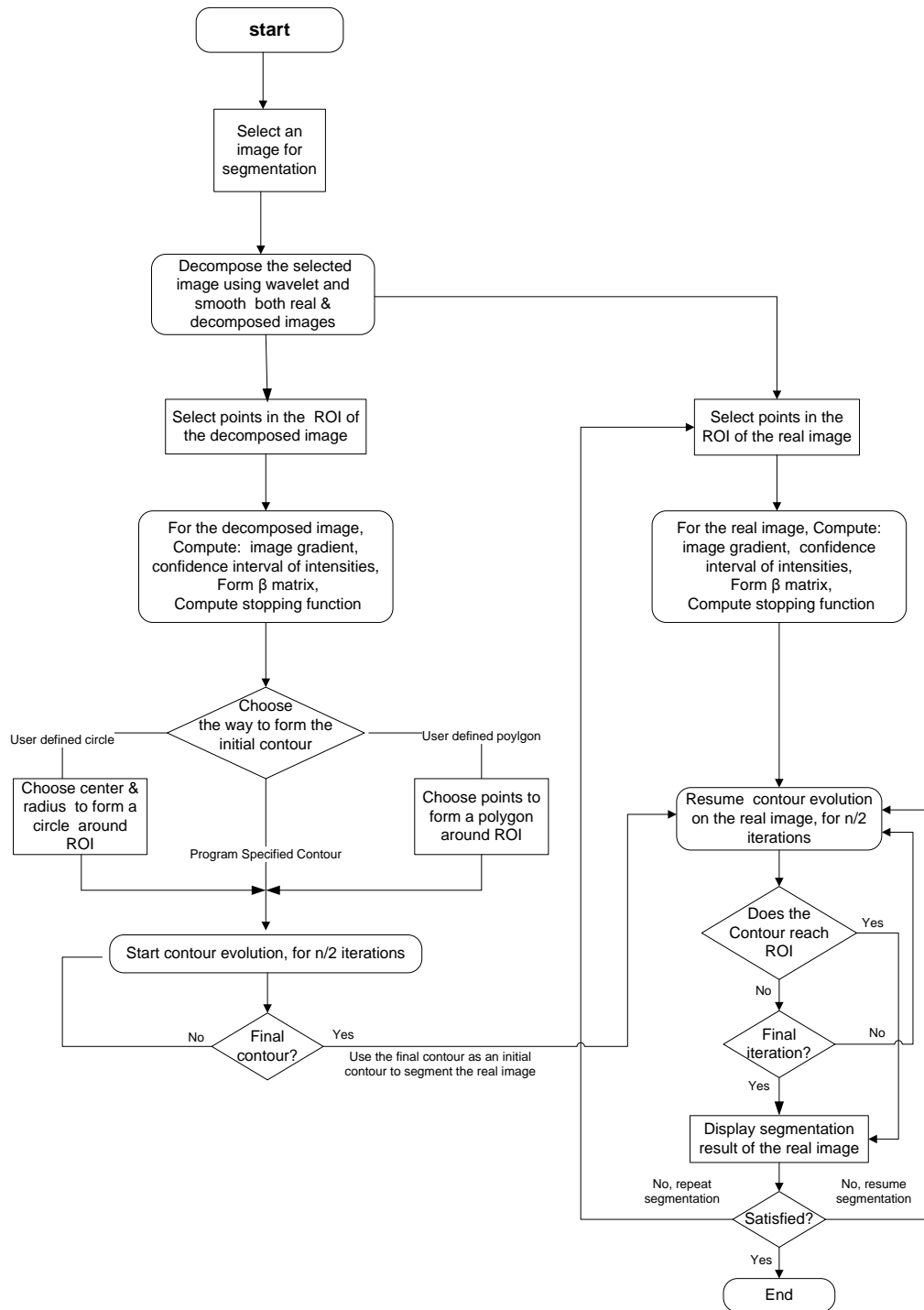
Figure.4. 3. Data Flow Diagram for the WACM Segmentation Technique

CHAPTER FIVE:

EXPERIMENTS AND RESULTS

5.1.   DEVELOPING AN INITIAL ACM MODEL:

Our results were obtained using the system proposed by Li et.al. [49]. The system was implemented in Matlab7.5.0 (R2007b) to gain familiarity with active contour models and its different controlling parameters. The original stopping function of the contour at this step is illustrated below in eq.5.1.

$$g(|\nabla I|) = \frac{1}{1+|\nabla(G_\sigma * I)|^2}$$

5. 1

To test the performance of the system quantitatively, the following steps were implemented:

1. Gaussian white noise, with a signal to noise ratio (SNR) =10dB, was added to a 512x512 synthetic image to produce image 5.1(b).

2. In order to reduce the noise in the input image which can lead the contour to false objects, the noisy image was smoothed with a Gaussian filter having a size of 15x15 pixels and a standard deviation σ = 1.5 (see figure. 5.1©).

(a)   (b)   (c)
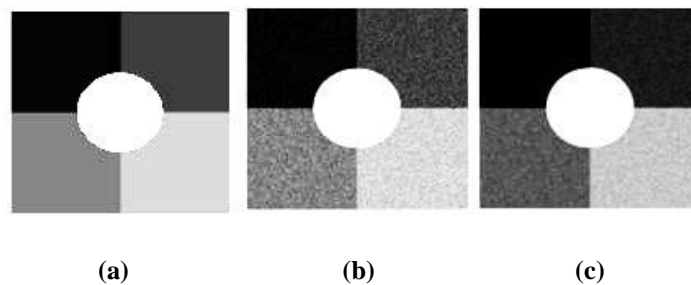
Figure.5.1. 512x512 Synthetic Image: (a) Original, (b) Noisy (SNR=10 dB), (c) Smoothed

3. The gradient of the smoothed image is calculated in order to form the stopping function of the evolving contour using eq.5.1; this function is used to stop the active contour when it reaches the edge of the desired object in the image since this function has its minimum value (approximately zero) on the edges.

4. An initial contour was specified around the region of interest in the input image. The specified contour deforms automatically and stops when it reaches the desired object boundaries.

In the developed program, the user has three options to choose from to select the initial contour which are:

i.   A Polygon Initial Contour; in which the user should specify a number points on the image using the mouse curser to form a polygon around the region of interest in the image.

ii.   A Circle Initial Contour; in which the user should specify a center and a radius of a circle on the image using the mouse cursor to let the program form a circle initial contour around the region of interest in the image.

iii.   A Program Specified Initial Contour; in which the program itself defines an initial contour around the region of interest in the image.
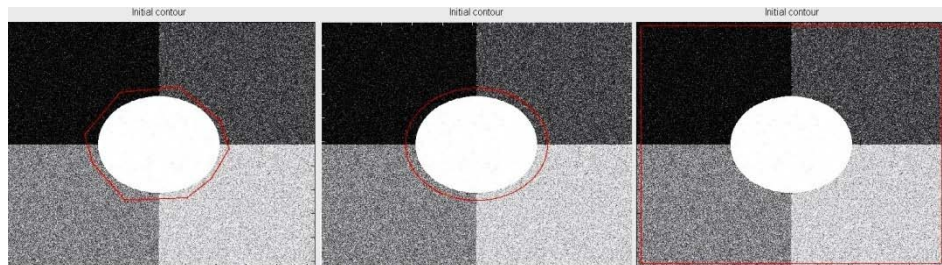
Figure.5.2. Initial Contour (a) Polygon, (b) Circle, (c) Program Specified

5.   After the initial contour is created, it starts evolution until it reaches the edge of object of interest in the image (see figure.5.3 where the synthetic image in figure5.1(b) is scaled to 128x128 and then segmented using a user-specified polygon initial contour around ROI):
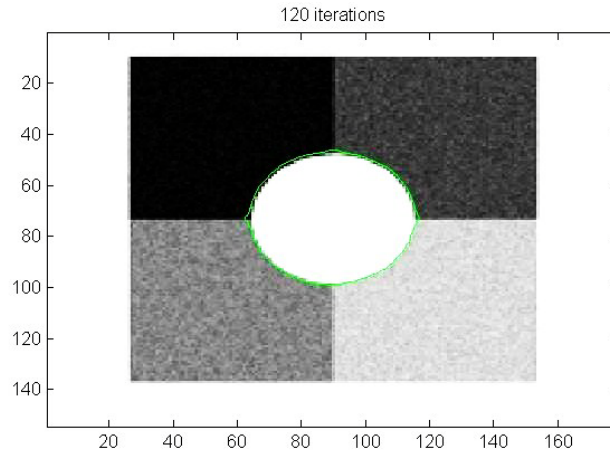
Figure.5.3. Scaled Segmented Image

The reason why the size of the image in figure 5.1(b) is rescaled to its ¼ before segmenting it refers to the fact that the size of this image is big. This means that the segmentation process of this image needs a large number of computations to be done by the algorithm in order to deform the contour. This number of calculations needs a lot of time, which means that the deformation process of the contour will be slow, i.e. the segmentation time will be too long.

After modifying the algorithm in the coming sections, it will be easy to segment the original image in figure.5.1(b) without rescaling it. In figure.5.4, the result of segmenting the original image in figure.5.1(b) without rescaling it, before the segmentation process started, and using the initial algorithm is shown. This process was done in order to compare its result with the future results after modifying the current segmentation algorithm.
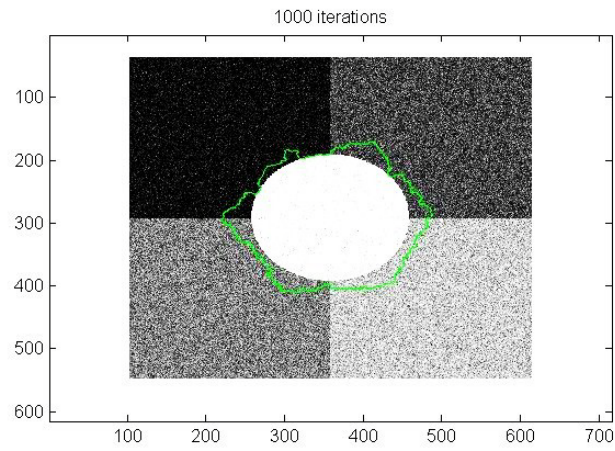
Figure.5.4. Result of Segmenting 512x512 Image Using The Initial Code

In figure.5.5, the data flow diagram describes the steps in how the initial algorithm works. This algorithm needs to be improved in order to increase its efficiency and this is our mission in the following sections.
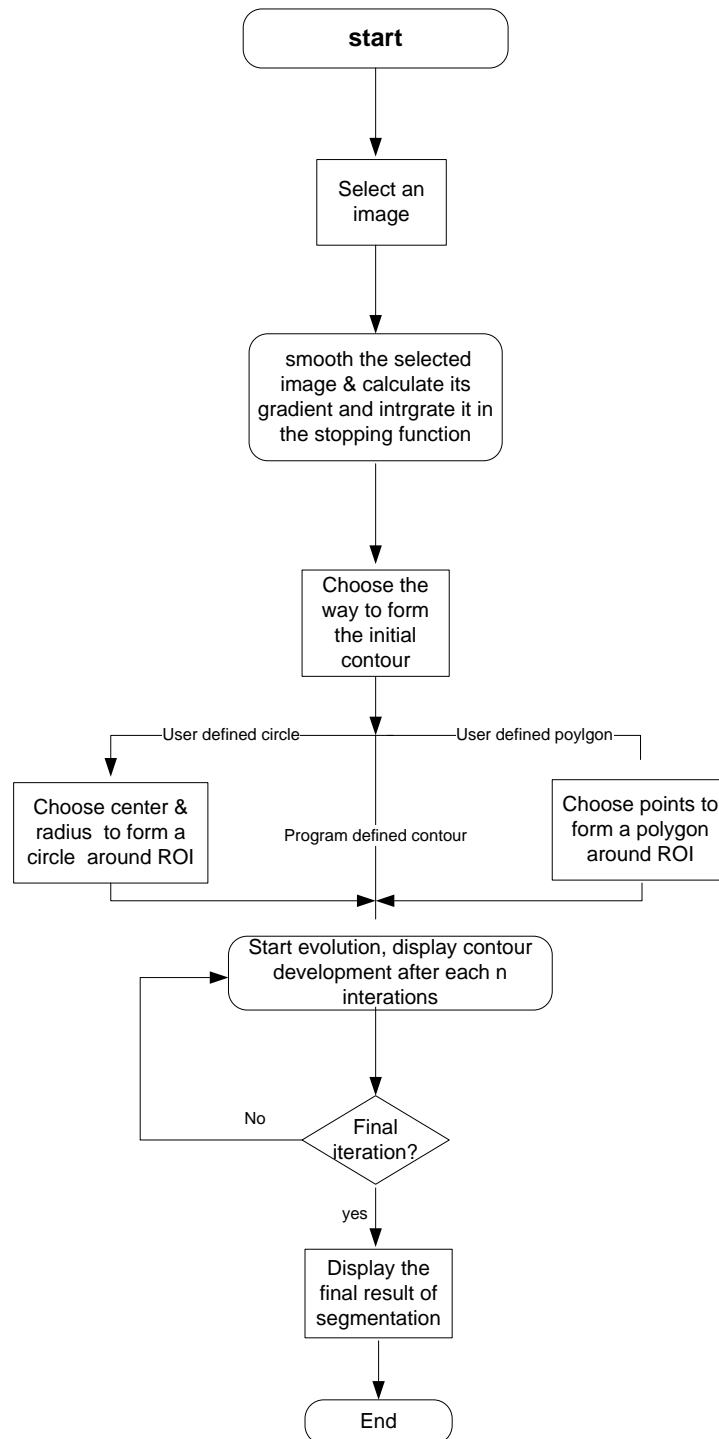
Figure.5.5. Data Flow of the Initial ACM Segmentation Algorith

5.2.   INCORPORATING PRIOR INFORMATION:

As noticed in section 5.1; the final result of segmentation is inaccurate or missing the real boundary, especially, when the input image is noisy. The reason for this bad result is that the noise in the input image leads the contour to converge to false edges. To solve this problem; number of points around the boundary of the region of interest (ROI) are manually selected to generate a training set. This set will form the points of interest (or samples). It needs to be further analyzed to discard some outliers since the selection of process is effectively subjective. After the analyzing the set of points, an intensity interval is obtained by applying some statistical techniques to the collected data. These techniques are discussed in detail in section (4.2.1). The formed intensity interval contains the pixel-range in which the region of interest (ROI) is situated.

As an example, the previous process was applied on the image in figure5.1(b) to segment the circle shape in it. The intensity values of the chosen points around the ROI were [253, 251,255,204,255,213]. After applying statistical analysis to the previous set using equn.4.7 with a critical value (c=0.98), the remaining intensity values has been limited to [253, 251,255,255,213] as result the initial intensity interval is [211,255]. By applying equn.4.9 on the obtained intensity interval using a degree of belief α=0.02, the remaining intensity values was limited to [253,251,255,255] which means that the final intensity interval became [251,255].

After getting the intensity interval, a matrix λ is formed with its dimensions are identical to the input image dimensions. This matrix should contain ones in each pixel where the intensity value of its peer pixel in the input image is within the intensity range of the intensity interval formed previously. The remaining pixels of this matrix are set to zero. After obtaining (λ) matrix, it is smoothed by a Gaussian filter. The result of this process is the matrix (β) which contains the location of the desired region of interest (ROI) extracted from the input image. Figure 5.5 shows an image mapping the resulting λ and (β) matrices of the previous example.
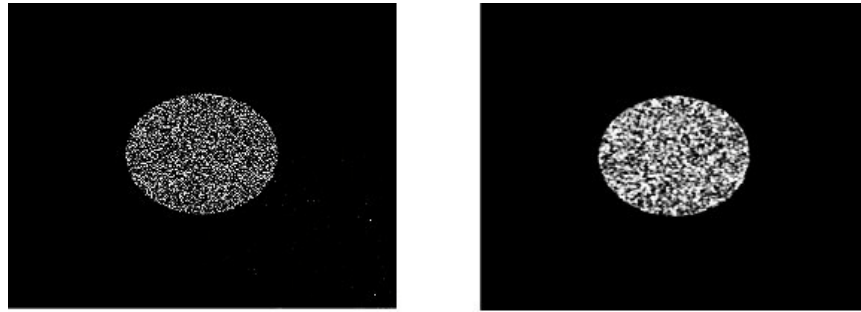
Figure 5.6. (Left) An Image Mapping λ matrix, (Right) An image Mapping β matix

In the next step, each point in this matrix (β) in multiplied by its peer point in the image gradient-matrix ($|\nabla(G_\sigma * I)|^2$), the resulting matrix is used to form the new stopping function g according to eq.5.2.

$$g(|\nabla I|) = \frac{1}{1+\beta(x)\bullet|\nabla(G_\sigma *I)|^2}, \quad \beta(x) = G_\sigma * \lambda(x) \qquad 5.2$$

This modification on the stopping function of the active contour is expected to increase its speed of convergence to the edges of the region of interest (ROI), since the stopping function - after this modification – will no longer have sharp edges except the edges of the (ROI), see figure 5.7, and this will force the contour to reach the edge in smaller period of time than it did before.

(a)   (b)
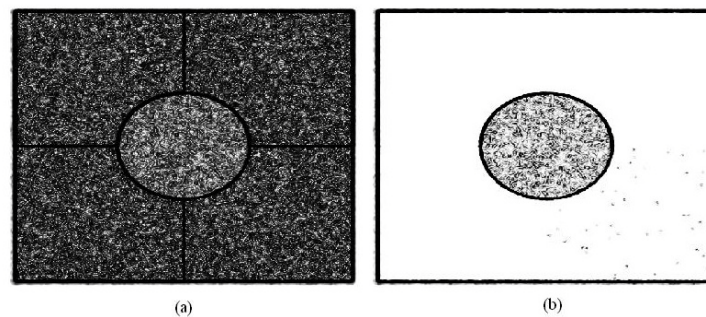
Figure.5.7 An Image Mapping the Stopping Function of the Segmented Synthetic Image (Figure.5.1(b)). (a) Using Image Gradient Only (b) Incorporating Prior Information

Steps of forming the stopping function with incorporating prior information are summarized below:

1.   Load an input image and smooth it.

2.   Choose a set of points on the borders of the region of interest (ROI) in the input image.

3.   Create a confidence interval containing the range of intensities of the region of interest (ROI) using eqs.4.7 - 4.9.

4. Form a matrix λ with dimensions identical to the input image dimensions, this matrix contains ones in each pixel where the intensity value of its peer pixel in the input image is within the intensity range of the intensity interval formed using prior information, and the remaining pixels of this matrix are set to zero.

5. Form matrix β by smoothing matrix λ.

6. Calculate the gradient matrix of the input image and smooth it.

7. Form the new stopping function using eq.5.2.

The result of segmentation with incorporating prior information to the stopping function is excellent when comparing it to the previous method; the speed of convergence to the edges of the region of interest is noticeably increased. Recall the poor result in figure 5.4 (no convergence to the ROI even after 1000 iterations which took more than 20 minutes).

The segmentation of the same image (figure 5.1(b)) was repeated again, but this time with incorporating prior information to the stopping function g. The result was excellent; the contour had converged to the edge of (ROI) in 3 minutes and 45 seconds after 180 iterations. The result of re-segmenting the noisy synthetic image in figure 5.1(b) with incorporating prior information is shown in figure.5.7 below.
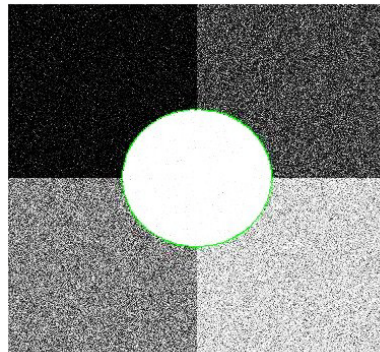
Figure.5.8. Segmentation of Noisy 512x512 Synthetic Image
With Incorporating Prior Information to the Stopping Function

There are two main issues which have a great influence on the speed of convergence of the active contour to the right edge with a minimum time, these factors are:

1.   The educated choice of the location and number the points on the boundaries of the (ROI) in the image which are used to obtain a confidence interval in order to form β matrix, (i.e. the best confidence interval, the best stopping function, which means, the most convergence efficiency).

2.   The educated way of specifying the initial contour (i.e. as the initial contour is closer to the region of interest, it needs fewer iterations to converge to the right edge which means a shorter convergence time).

These factors have a great influence on the active contour (snake) performance; they need only a little bit more accuracy from the user. It is recommended to put them in consideration when using the algorithm to segment an image by specifying the initial

contour as close as possible to the ROI and choosing the points, which are used to form β

matrix, inside the ROI.

5.3.   Introducing A NEW Stopping Function:

The stopping function (shown in eq.5.2.) can be enhanced more in order to make

the active contour converge faster and faster. This can be achieved by using the function

(e^x) in the denominator of the stopping function in eq.5.2. By applying this change, we'll

benefit from the mathematical properties of the function (e^x) in increasing the speed of

the stopping function. The following equations states how we can use the function (e^x)

to improve the speed of the current stopping function.

$$g(|\nabla I|) = \frac{1}{1+e^{\beta(x)\bullet M}}, \quad M = |\nabla(G_\sigma * I)|^2 \qquad 5.3$$

If we expand the term $(e^{\beta(x)\bullet M})$ using Taylor series expansion, this term will become

as the following:

$$e^{\beta(x)\bullet M} = 1 + \beta(x) \bullet M + \frac{\beta(x)^2 \bullet M^2}{2!} + \frac{\beta(x)^3 \bullet M^3}{3!} + \frac{\beta(x)^4 \bullet M^4}{4!} + \cdots \qquad 5.4$$

As a result of this expansion, eq.5.3. becomes as the following:

$$g(|\nabla I|) = \frac{1}{2 + \beta(x) \bullet M + \frac{\beta^2(x) \bullet M^2}{2!} + \frac{\beta^3(x) \bullet M^3}{3!} + \frac{\beta^4(x) \bullet M^4}{4!}} \qquad 5.5$$

In eq.5.5, the expansion was stopped at the 4th power because there is no speed improvement of the snake after this value. This result was obtained after running the algorithm for several times.

Table 5.1 shows the performance of the active contour (snake). The results in the table were obtained after performing a test over the ACM algorithm using the eqs.5.2, 5.3, and 5.5 respectively in the stopping function. The target of this test was to determine the most suitable stopping function for the ACM using an initial contour as "program specified contour".

The test was performed using 512x512 synthetic images and the initial contour used in each run of the program was chosen to be a "program specified contour" around the whole input image. Also, the confidence interval, obtained after prior information analysis, was fixed for each image tested by the ACM algorithm using different stopping functions. The reason why this confidence interval was fixed is that; we wanted to test the effect of changing the stopping function, of the ACM, on the speed of its convergence for each image tested. This required us to fix the value of β matrix.

Tested Input image	Convergence speed using priors only		Convergence speed using priors & e^x		Convergence speed using priors & truncated e^x	
	# of itrs.	Seg. time (sec.)	# of itrs.	Seg. time (sec.)	# of itrs.	Seg. time (sec.)
Figure.5.9. (a)	780	794	1070	1070	780	778
Figure.5.9. (b)	800	790	1070	1069	800	816
Figure.5.9. (c)	690	693	930	941	690	723
Figure.5.9. (d)	660	712	1060	1072	660	728
AVG. contour speed (Sec./100 itrs.)	102		100.5		104.5	

Table 5.1 Results of Segmenting Synthetic Images Using a "Program Specified" Initial Contour

From table 5.1, we conclude that; if we are using the initial contour to be "program specified", the best choice for the stopping functions of the ACM is to select the one which incorporates prior information but without using the exponential (eq.5.2.) to accomplish this task. In this case, we can get the fastest speed of convergence of the snake in terms of time and number of iterations. The input images used in the above test are shown in (figure.5.9).
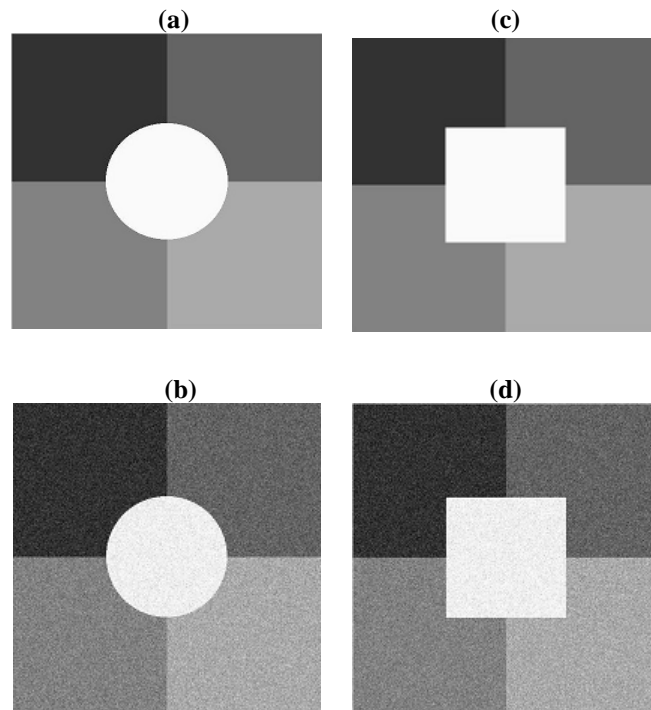
Figure.5. 9. 512x512 Synthetic Images

The same test was repeated again using the same test images. This time, the initial contour was chosen to be a "user-specified polygon". Using this kind of initial contours, the user is asked to choose points around the ROI in the image. These points are used to form a contouring polygon around the ROI. Once this is done, the contour starts deforming until it reaches the edges of the ROI and stops there. The same conditions as the previous test apply here. Results of this experiment are shown in table 5.2.

Tested Input image	Convergence speed using priors only		Convergence speed using priors & e^x		Convergence speed using priors & truncated e^x	
	# of itrs.	Seg. time (sec.)	# of itrs.	Seg. time (sec.)	# of itrs.	Seg. time (sec.)
Figure.5.9. (a)	170	196	170	196	170	196
Figure.5.9. (b)	280	324	280	324	210	243
Figure.5.9. (c)	140	136	180	176	140	135
Figure.5.9. (d)	180	174	250	245	180	173
AVG. contour speed (Sec./100 itrs.)	108		109		107	

Table 5.2 Results of Segmenting Synthetic Images Using a "User- Specified Polygon" Initial Contour

From the results above, we conclude that; if our choice for the initial contour is a "user-specified polygon," then, the best selection of stopping functions for the active contour (snake) is using priors & truncated e^x in the stopping function (eq.5.5) to accomplish this task. In this case, we can get the fastest speed of convergence of the snake in terms of time and number of iterations.

The same test was repeated for the third time, but now after choosing the initial contour to be a "user-specified circle". Using this kind of initial contours, the user is asked to choose a center and a radius of a circle around the ROI in the input image. Once this is done, a circle appears contouring the ROI. It starts deforming until it reaches the edges of the ROI and stops there. The same conditions as the previous tests apply here. Results of this experiment are shown in table 5.2.

Tested Input image	Convergence speed using priors only		Convergence speed using priors & e^x		Convergence speed using priors & truncated e^x	
	# of itrs.	Seg. time (sec.)	# of itrs.	Seg. time (sec.)	# of itrs.	Seg. time (sec.)
Figure.5.9. (a)	400	350	525	462	350	308
Figure.5.9. (b)	400	348	425	373	400	348
Figure.5.9. (c)	1100	940	1260	1065	910	793
Figure.5.9. (d)	1150	999	1320	1150	1000	875
AVG. contour speed (Sec./100 itrs.)	86.5		86.4		87	

Table 5.3 Results of Segmenting Synthetic Images Using a "User- Specified Circle" Initial Contour

From table 5.3, we conclude that; if we are using the initial contour to be a "user-specified circle," the best choice for the stopping function of the active contour (snake) is selecting the one which incorporates priors only (eq.5.2.) to accomplish this task, except when the shape of the ROI square-like. In this case, it is recommended to use the stopping function which incorporates priors and uses the truncated e^x (eq.5.5.) to successfully do this task.

The results of the previous tests above showed that the best initial contour used around the ROI of the snake is the "user-specified polygon"; This initial contour can be used for any shape of the ROI and it gives excellent results. The "user-specified circle" initial contour gives very good results, except when the ROI is square-shaped, in this case, this type of initial contour is not recommended to be used. Using a "program-specified" initial contour, gives very good results but it needs more time than other

techniques to converge to the ROI. This type of initial contours   is recommended to be use when the ROI is big.

In figure.5.10, the resulting segmented images of the previous tests are shown. They are arranged according to the initial contour used in the segmentation process of each image.

program specified	User specified polygon	User specified circle
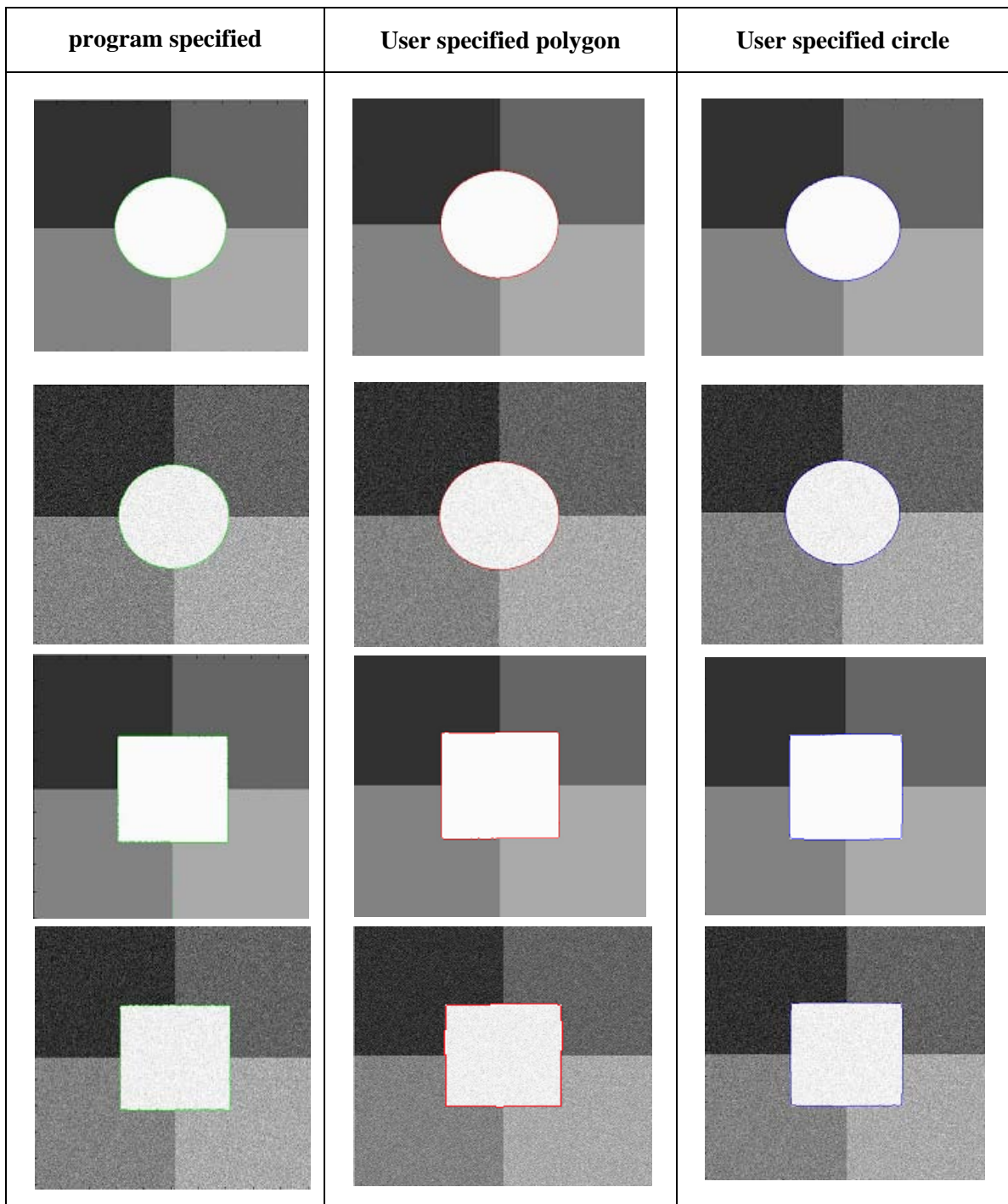
Figure 5.10. 512x512 Segmented Synthetic Images

Figure 5.11, shows the data flow of the program after the modification in this section:
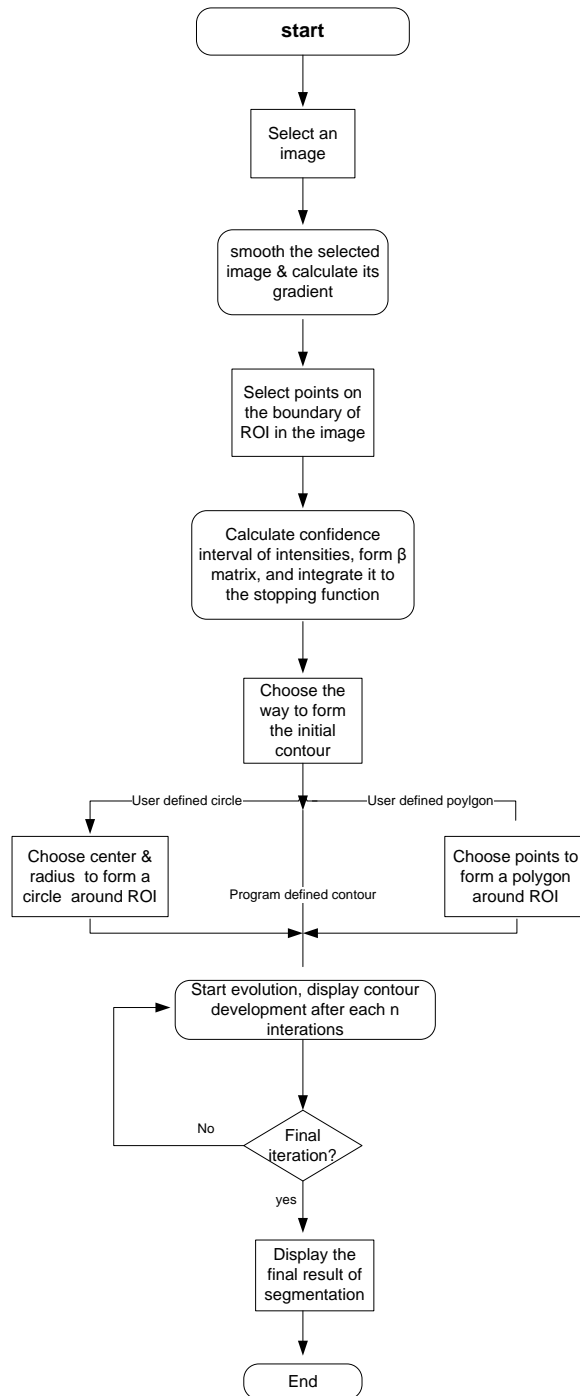
Figure5.11 Modified Data Flow Diagram of The Segmentation Algorithm

5.4   THE WAVELET-BASED ACM MODEL:

From previous experiments, we can find that the speed of the active contour is approximately one second per iteration. This speed can be improved more by decomposing the input image using wavelet transform and then running the active contour to segment ROI in the sampled image. The final contour of this process is used as an initial contour for the next step in which the real image is segmented. This process is expected to increase the speed of the active contour by a noticeable ratio.

The purpose of the next test is to evaluate the performance of the active contour after the new enhancement (using wavelet) is applied. The image used in this test is IM78 (see figure 5.14). After adding the new enhancement to the program, it was run 30 times using the input image (IM78). After each 10 runs of the program, the stopping function was changed (in order to test the enhanced program using the three proposed stopping function in eqs. 5.2, 5.3, 5.5). The results of this experiment are shown in table5.4.

Stopping Function		Convergence speed using priors only	Convergence speed using priors & e^x	Convergence speed using priors & truncated e^x
Program Speed (sec./100 iterations)	1	15.215	16.588	16.31
	2	16.421	14.389	14.785
	3	18.429	16.738	14.490
	4	15.696	17.190	14.187
	5	14.689	15.512	14.659
	6	15.491	14.368	14.289
	7	14.321	16.982	14.250
	8	14.806	14.356	14.736
	9	15.565	14.596	13.532
	10	17.334	14.279	13.016
Average Speed sec./100 Itr.		**15.797**	**14.2**	**14.423**
Time Reduction		**0**	**-10.11%**	**-8.7%**

Table 5.4 Active Contour Speed After Using Wavelet in the Developed ACM

By using wavelet to down-sample the medical image and then start segmenting the sampled image (phase1), the algorithm speed has increased by more than 5 times. This process does not affect the accuracy of the program (see figure 5.12).

After getting the final contour of the previous step, it is used as an initial contour for segmenting the real input image (phase2). Applying this technique has decreased the numbers of computation done by the algorithm and this improvement has increased the speed of the contour evolution. Previously, it took the algorithm 104 seconds to perform 100 iterations, while now, the time required to perform this number of iteration has dropped to 85 seconds only. For example, suppose that the algorithm is required to perform 200 iterations in order to allow the active contour to reach the ROI, if the first

100 iterations are performed using the sampled input image, the time needed to do this step is only 15 seconds. The next 100 iterations are to be performed using the final contour of the previous step to segment the real 512x512 input image. This step requires 85 seconds to accomplish it. The total time required for the whole segmentation process (200 iterations) is 100 seconds. Recall that before this enhancement, the time needed to perform 200 iterations was 208 seconds. This means that, by applying the new technique, we have got an improvement of 43 % in the speed of convergence of the snake.

(a)   (b)
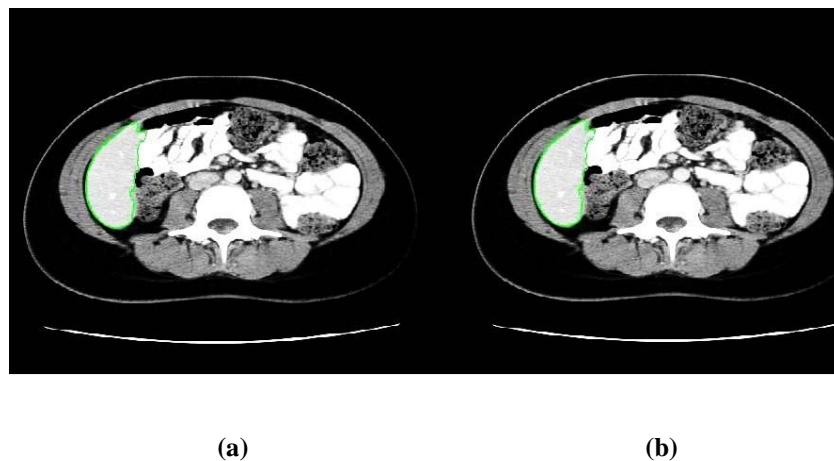
Figure 5. 12   Segmentation Result Using Wavelet (a) Segmented Non-sampled Image, Speed of Snake=104 sec./100 itr. (b) Segmented Sampled Image, Speed of Snake=15.33 sec./100 itr.

The new technique was tested on the medical image named IM78 (see figure 5.14) and compared with the previous segmentation technique (see sections 5.2 and 5.3). Using the previous technique, the segmentation process was accomplished after the algorithm performed 70 iterations with the rate of 108 sec./100itrs. which means that the process

was accomplished after 76 seconds. Now, the new technique is applied on the same image. This technique has two phases. In the first phase, the image is sampled using wavelet and then segmented by running the algorithm to perform 35 iterations with the rate of 15 sec. /100 itrs (see table 5.4). Then, the second phase started by using the final contour of the previous phase as an initial contour for segmenting the real input image by performing another 35 iterations by the algorithm with the rate of 108 sec. /100 itrs. (see table 5.2). The time consumed to accomplish the whole process was 43 seconds which means that, by using the new technique, we got 43% improvement in the speed of the snake.

Assuming that the number of iteration required to reach the ROI using the snake is denoted by (n), we can calculate the improvement (η) in the active contour speed which we got by applying the new technique as follows:

$$\eta = \frac{\left(\left(^{108}/_{100} * n\right) - \left(\left(^{108}/_{100} * ^{n}/_{2}\right) + \left(^{15}/_{100} * ^{n}/_{2}\right)\right)\right)}{^{108}/_{100} * n} = 43 \ \%$$

The following notes are clearly observed when using this technique:

- The active contour speed is clearly increased by a factor depending on the ratios of the number of iterations used in each phase.

- The speed of the contour depends on the stopping function used, and it is the maximum when using the stopping function which incorporates prior & uses the truncated e^x (eq.5.3) to stop the snake on the edges of ROI (see table.5.4).

- This method requires the user to define the confidence interval (see section 5.2) twice; the first time is when tending to segment the sampled input image (phase1) and the second time is when tending to segment the real input image (phase2). The new data flow diagram of the program is shown in figure 5.12.

start

Select an image for segmentation

Decompose the selected image using wavelet and smooth both real & decomposed images

Select points in the ROI of the decomposed image

Select points in the ROI of the real image

For the decomposed image, Compute: image gradient, confidence interval of intensities, Form β matrix, Compute stopping function

For the real image, Compute: image gradient, confidence interval of intensities, Form β matrix, Compute stopping function

Choose the way to form the initial contour

User defined circle

User defined poylgon

Choose center & radius to form a circle around ROI

Choose points to form a polygon around ROI

Program Specified Contour

Resume contour evolution on the real image, for n/2 iterations

Start contour evolution, for n/2 iterations

Does the Contour reach ROI

Yes

No

No

Final contour?

Yes

No

Final iteration?

No

Use the final contour as an initial contour to segment the real image

Yes

Display segmentation result of the real image

No, repeat segmentation

No, resume segmentation

Satisfied?

Yes

End

Figure.5. 13 Data Flow Diagram of the ACM Model Using Wavelet

5.5.   APPLICATION OF WACM ALGORITHM ON SIMULATED DATA IN MEDICAL IMAGING:

In this section, the developed program was used to segment a set of 512x512 real DICOM CT images in order to examine its performance. The results of the previous tests were taken into account in this experiment. So, the initial contour used in this experiment was the "user-specified polygon," the stopping functions in eqns.5.2, 5.3, and 5.5 were used respectively in the segmentation process of each image. Also, same initial contour and β matrix are used for each image. The DICOM images used in this test are shown in figure 5.14.
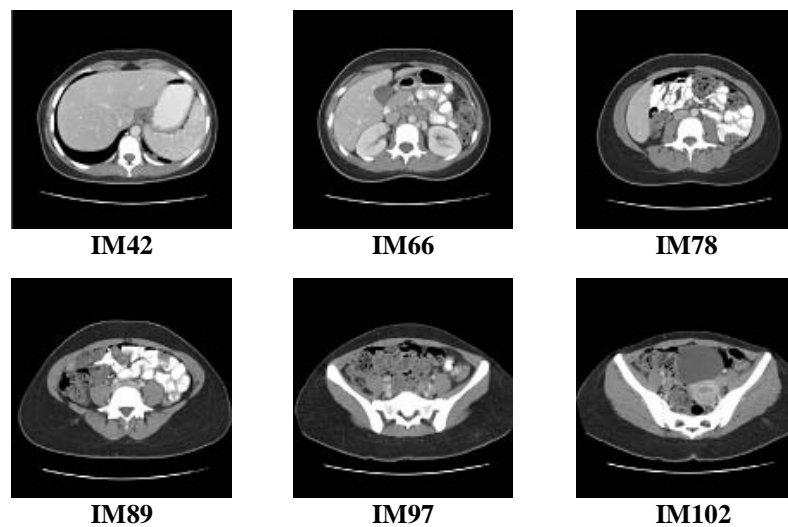
Figure .5.14 512x512 DICOM CT Images

Table 5.5, shows the results of segmenting the DICOM images of figure 5.14 using "user-specified polygon" as an initial contour without using wavelet:

| DICOM image name	Convergence speed using priors only		Convergence speed using priors & e^x		Convergence speed using priors & truncated e^x	
	# of itrs.	Seg. time (sec.)	# of itrs.	Seg. time (sec.)	# of itrs.	Seg. time (sec.)
IM42	80	80.3	80	81	80	81
IM66	80	79	80	79.5	80	83.6
IM78	110	113	100	105	100	101
IM89	80	82	80	80.4	80	80.4
IM97	240	241	240	225	240	228
IM102	70	72	70	69	70	63
AVG. contour speed	**99** sec./100 itrs.		**102** sec./100 itrs.		**98** sec./100 itrs.	

Table 5.5 Results of segmenting DICOM images using "User- Specified Polygon" Initial Contour

After incorporating wavelet to the algorithm, we got the following results for segmenting the same images:

DICOM image name	Convergence speed using priors only		Convergence speed using priors & e^x		Convergence speed using priors & truncated e^x	
	# of itrs.	Seg. time (sec.)	# of itrs.	Seg. time (sec.)	# of itrs.	Seg. time (sec.)
IM42	80	46.5	80	46.2	80	46.3
IM66	80	46	80	45.5	80	47.6
IM78	110	65.6	100	59.6	100	57.8
IM89	80	47.5	80	46	80	46
IM97	240	140	240	129.6	240	131.3
IM102	70	41.6	70	39.5	70	36.6
AVG. contour speed	**58.6** sec./100 itrs.		**56.4** sec./100 itrs.		**56.25** sec./100 itrs.	
Speed Improvement	**41 %**		**44.7 %**		**42.6 %**	

Table 5.6 Results of segmenting DICOM images using WACM Algorithm

As noticed from table 5.6, the average speed improvement using the new technique (WACM) is approximately 43%. The maximum improvement of the contour speed is obtained when incorporating prior information and full e^x to the stopping function of the snake. Figure 5.15 shows the resulting segmented DICOM images.

| **IM42** | **IM 89** | **IM66** |

| **IM78** | **IM97** | **IM102** |
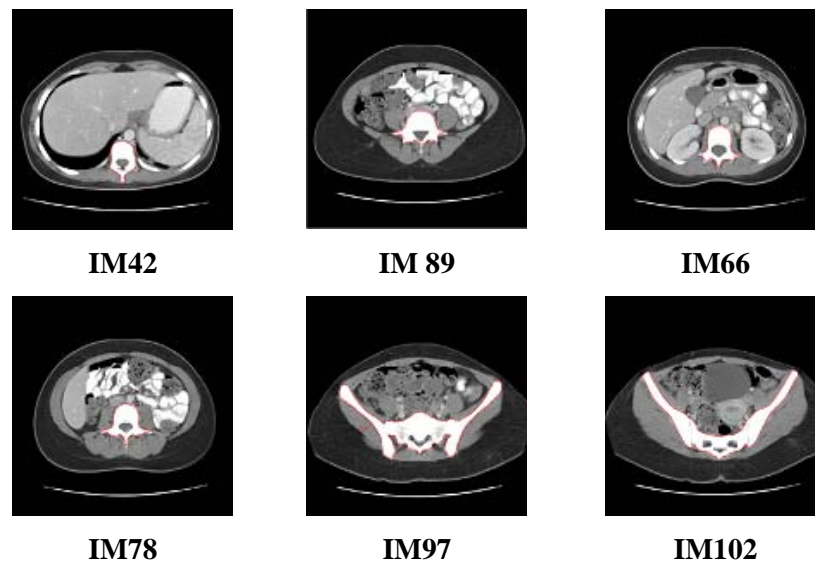
Figure.5.15 512x512 Segmented DICOM Images

5.6   EVALUATING THE ALGORITHM ACCURACY:

Accuracy of the algorithm is an important measure which helps the user to decide if the algorithm suits his/her application. To evaluate the accuracy of WACM algorithm, the segmented areas of synthetic images in figure 5.10 were compared with the area of the actual objects. Suppose we want the obtain the segmentation accuracy of the image in figure 5.16, to do this, we find the number of pixels in both the areas segmented

or unsegmented by error and add them together. Then, the obtained result is divided by

the actual number of pixels   in the ROI (see eq.5.6)

ROI A0
Contour
Unsegmented area in ROI (A1)
Segmented area out of ROI (A2)
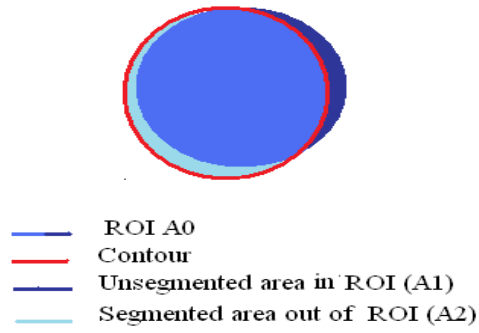
**Figure 5.16 Segmentation accuracy test**

$$Q = \left(1 - \frac{1}{2}\left[\frac{N(A_1)+N(A_2)}{N(A_0)}\right]\right) * 100\%$$ 5.6

where N(.) is the number of pixels, A_0 is the area of ROI, A_1 is the unsegmented area in

the ROI, and A_2 is the segmented area out of ROI.

Applying the previous formula of the synthetic images in figure 5.10, we got the

following results for the algorithm accuracy.

Image	Program Specified Initial Contour	Polygon Initial Contour	Circle Initial Contour	
(a)	92.0 %	85.7 %	88.7 %	
(b)	91.3 %	84.5 %	89.0 %	
(c)	90.0 %	89.0 %	85.6 %	
(d)	89.0 %	88.5 %	88.7 %	
Q Avg.	**90.6 %**	**86.75 %**	**88.0 %**	**88.45 %**

Table 5.7 Evaluating WACM Algorithm accuracy

5.7. GRAPHICAL USER INTERFACE (GUI):

A friendly graphical user interface was designed to facilitate the practitioner interaction with the algorithm. At the beginning, a welcome screen appears to identify the algorithm objective (figure 5.17-Left). Then, the user is asked to load an image to segment it (figure 5.17-Right).
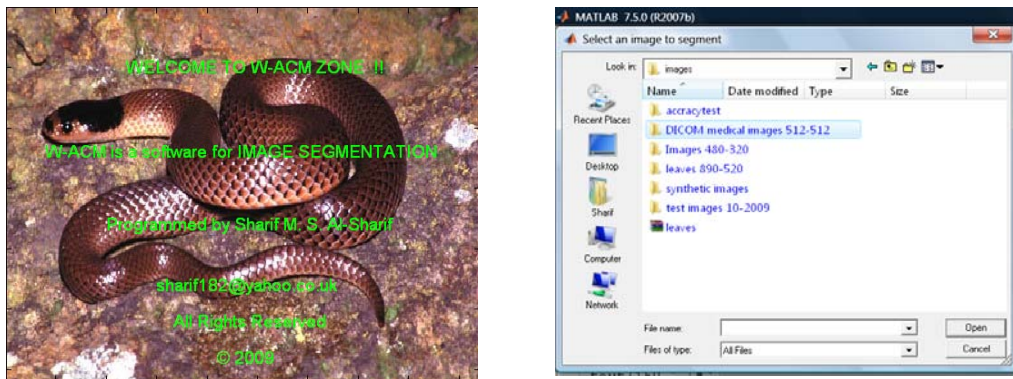

Figure 5 . 17. Program Initialization, (Left) Welcome screen, (Right) Request for loading an image to segment it.

After choosing the image, it is smoothed by a Gaussian kernel and decomposed using wavelets, then, the user is asked to choose a set of points in the ROI in order to form an intensity confidence interval (figure 5.18-a). After that, β matrix and image gradient are computed and the stopping function of the active contour is formed. Figure 5.18-b.

(a)   (b)
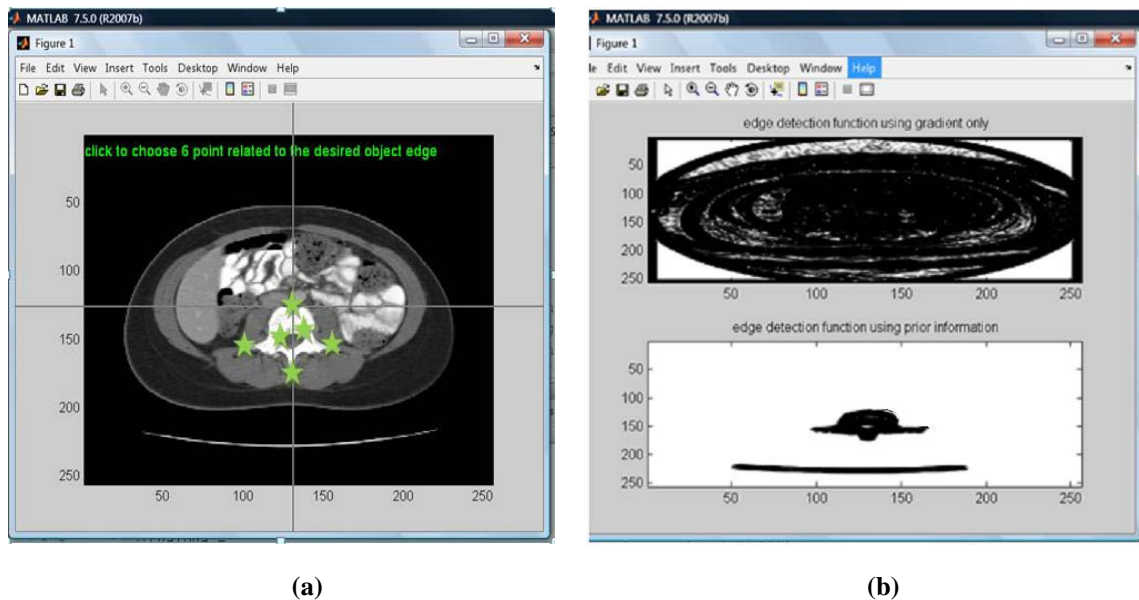
Figure 5. 18. Incorporating Priors (a) Choosing Points in the ROI, (b) Image of the Stopping Function

In order to start the segmentation process, an initial contour around ROI should be specified by the user (figure 5.19).

Figure 5. 19 An Interface Asking the User to Choose the Type of Initial Contour

The program offers the user the capability to specify one of the following initial contours: User-Specified Polygon around ROI (figure 5.20), User-Specified Circle around ROI (figure 5.21) and Program-Specified Contour around the whole image (figure 5.22).
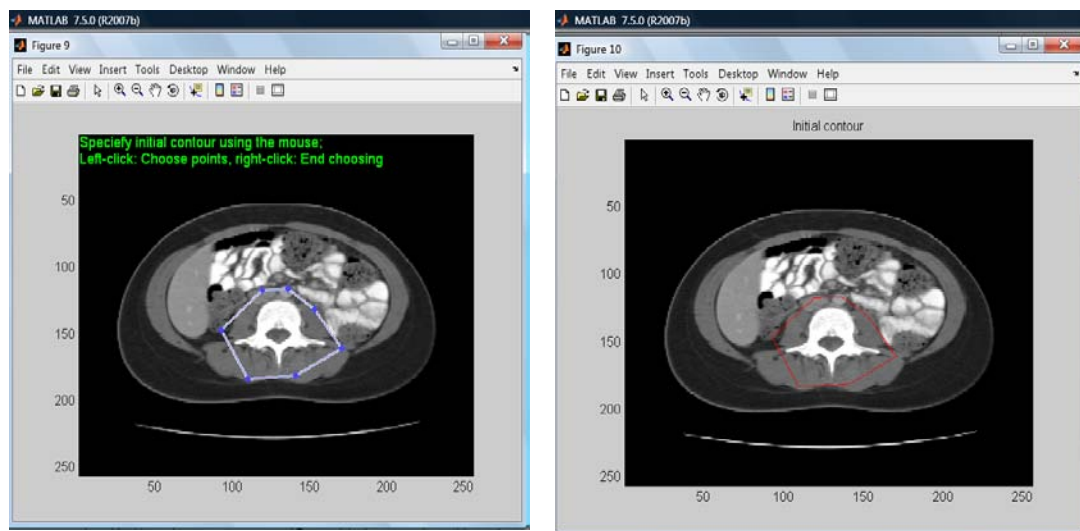
Figure 5 . 20 Specifying A Polygon Initial Contour around ROI
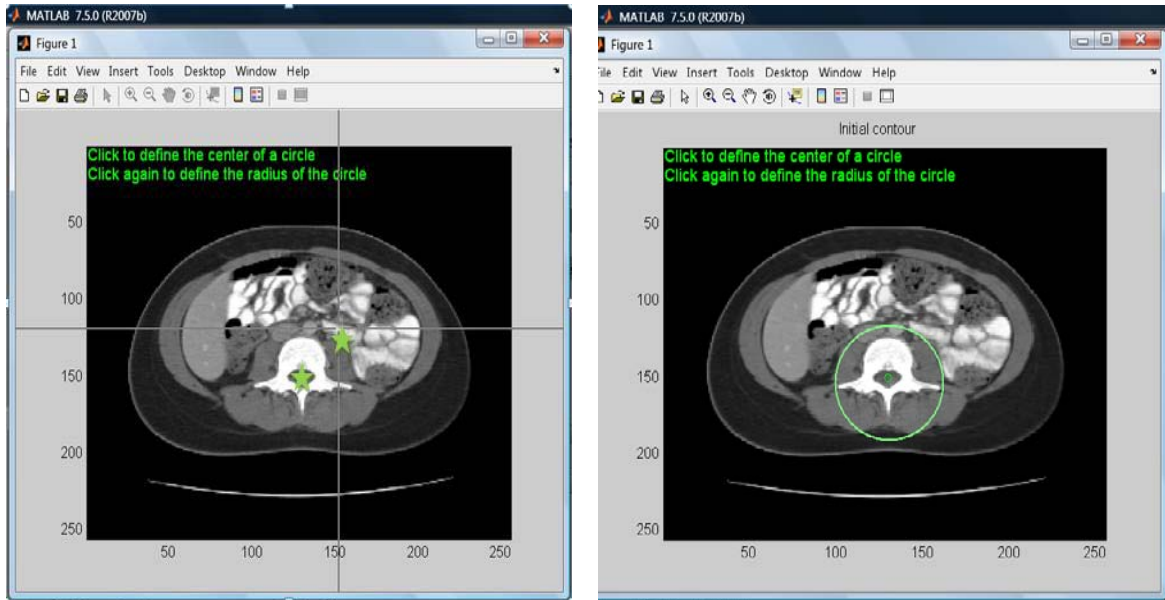
Figure 5 . 21 Specifying A Circle Initial Contour Around ROI
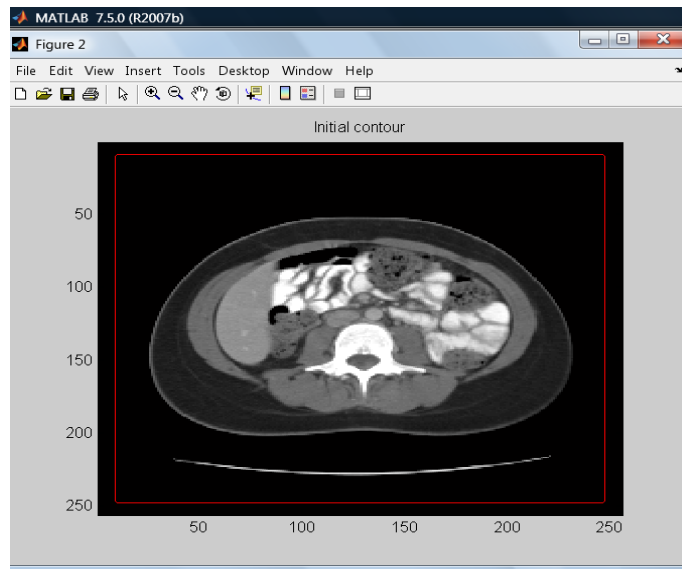
Figure 5. 22 A Program Specified Contour Around the whole image

After choosing the initial contour, it starts its evolution for n/2 iterations, where n is the total number of iterations required by the contour in order to reach ROI, this process is called Phase I (see figure 5.23).
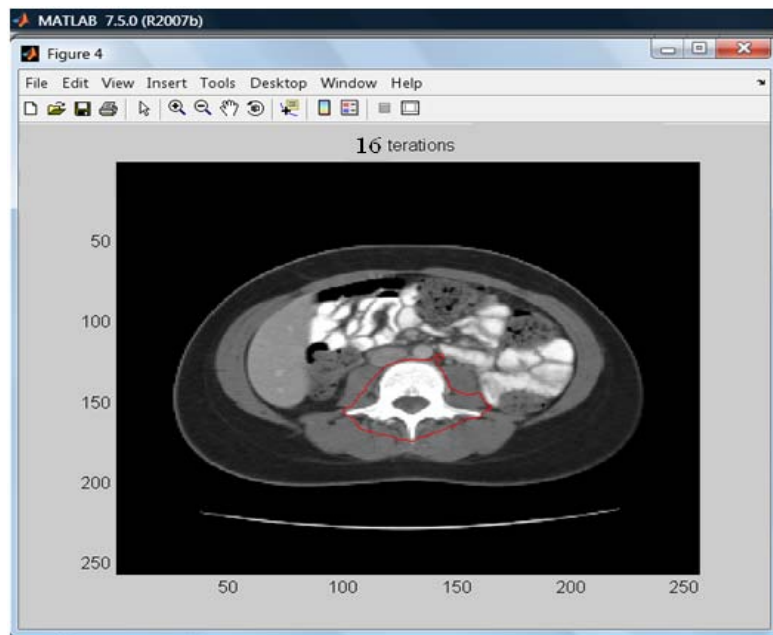
Figure 5. 23 Final Contour of Phase I

The final contour of the previous step is used as an initial contour to segment the real image; this process is called Phase II. Figure 5.24 shows the final result of the segmentation process.
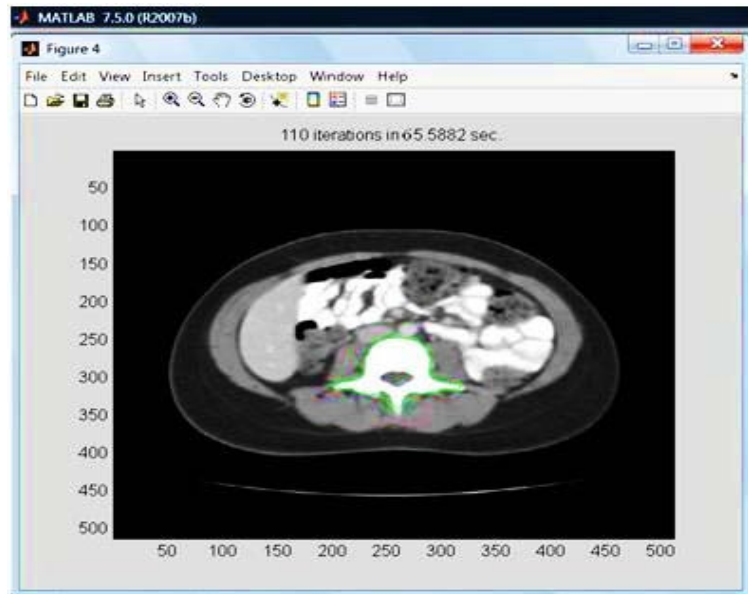
Figure 5. 24 Final Result of the Segmentation Process

Finally, the user is asked if he/she is satisfied with the segmentation result. If not, the program gives the user a choice to resume or repeat the segmentation process.

Figure 5. 25 User Satisfaction of the Segmentation Result

CHAPTER SIX

DISCUSSION AND CONCLUSIONS

6.1.   SUMMARY OF RESULTS:

The role of medical imaging has expanded beyond the simple visualization and inspection of anatomic structures. It has become a tool for surgical planning and simulation, intra-operative navigation, radiotherapy planning, and for tracking the progress of diseases.

Medical image analysis has become one of the most active areas of research these days; many important achievements have been addressed in this field which is vital for physicians who become highly dependent on the image information in order to give an accurate diagnose for diseases.

Computer processing and analysis of medical images covers a broad number of potential topic areas. One of the well known approaches in medical image analysis is Image Segmentation; its idea is to subdivide the image into regions in which each one contains components having the same properties. The goal of segmentation is to simplify and/or change the representation of an image into something that is more meaningful and easier to analyze. This approach is widely used in extracting the tumor areas from medical images as a first step in the therapy planning.

Many techniques in image segmentation were proposed. The most visible approaches brought to maturation during the 1980s and 1990s in terms of both methodology development and application were boundary finding strategies based on deformable model. This approach can be found in literature under different names such as snakes, active contours, surfaces or balloons; It is a deformable continuous curve consists of a set of control points connected by straight lines. Forces are applied upon the snake in order to control its shape. Its objective is to divide an image into a number of strongly correlated objects of reality. Shaping the image by fitting active contours is an interactive process in which an initial contour should be suggested by the user (should be as close as possible to the intended shape). The contour will be attracted to features in the image extracted by internal energy creating an attracter image.

In this work, three techniques for specifying the initial contour were proposed, these methods are; (1) User-Specified Polygon initial contour; in which the user should specify a number points on the image using the mouse curser to form a polygon around

the region of interest in the image. (2) User-Specified Circle initial contour; in which the user should specify a center and a radius of a circle on the image using the mouse cursor to let the program form a circle initial contour around the region of interest in the image. (3) Program specified initial contour; in which the program itself defines an initial contour around the region of interest in the image.

Sometimes, curve evolution becomes sensitive and unstable so that the final result in some cases will be inaccurate or missing the real boundary. To remedy this problem; a number of points on the boundary of the region of interest (ROI) are manually selected to generate a training set. This set will form the points of interest (or samples) and need to be further analyzed to discard some outliers since the selection is effectively subjective.

Within the GAC technique, the stopping function g plays a critical role and controls when the curve evolution will arrive at the boundary during the iterative approximation procedure where there is high image gradient (e.g. at a boundary) the value of g will be closer to zero; in homogeneous regions the value will be closer to 1. Thus, we can revise the stopping function according to the prior information where we wish the priors to affect the process of curve evolution. Our method was to modify the stopping function in order to make its value (around object boundary) closer to zero by employing the prior information while the curve is approaching to the boundary. This process was applied in three different ways in which the speed of convergence of the snake to the edges of the region of interest was noticeably improved.

The speed of the active contour can be improved more by decomposing the input image using wavelet transform and then running the active contour to segment ROI in the sampled image. The final contour of this process is used as an initial contour for the next step in which the real image is segmented. This process has increased the speed of the active contour by a noticeable ratio.

The developed model was then used to segment a set of 512x512 real DICOM CT images in order to examine its performance on real images. In this experiment, the program has given very good results, but it was needed to improve the snake speed more in order to reduce the segmentation time of the medical images. To solve this problem, Wavelet transform was used to down-sample the input image. The resulting image after down sampling was segmented by the snake. The final contour resulting from this process was used as an initial contour for the snake to segment the original (un-sampled) input image. This process has increased the speed of the snake very significantly.

In order to facilitate the use of the proposed model, a friendly graphical user interface (GUI) was designed. It starts by asking the user to choose an image to segment. Next, the selected image is loaded and the user is asked to choose a set of points on the edges of ROI. After that, the user is asked to choose the type of the initial contour and also to select points around the ROI in order to create it. Then, the evolution of the contour over the image is displayed after each n iterations. At the end of segmentation process, the final curve is displayed contouring the ROI in the image and the user is asked

if he/she is satisfied with the segmentation result and if he/she wants to continue or repeat segmentation of the current image, or if he/she wants to segment a new image.

6.2.   FUTURE RESEARCH DIRECTIONS:

The following research directions are expected to have promising results:

1.   Joining active contour and region growing segmentation techniques by using the final contour obtained by the snake to create an initial seed for the region growing segmentation technique.

2.   Performing parallel segmentation of two or more objects in an image at the same time using the active contour approach.

3.   Constructing a three dimensional object after segmenting a series of two dimensional images using active contour. The final contour obtained after segmenting each image can be used as an initial contour to segment the next one.

REFERENCES

[1] McInerney T. and Terzopoulos D. (1996), "Deformable Models in Medical Image Analysis: A Survey**,** Medical Image Analysis, **1**(2):91–108.

[2] Duncan J. S. and Ayache N. (2000), "Medical Image Analysis: Progress over Two Decades and the Challenges Ahead", IEEE Transactions on Pattern Analysis and Machine Intelligence. 22(1), January .

[3] Linda G. Shapiro and George C. Stockman (2001): "Computer Vision", pp 279-325, New Jersey, Prentice-Hall, ISBN 0-13-030796-3.

[4] Kass, M., Witkin, A. and Terzopoulos, D. (1988). "Snakes: Active contour models". International Journal of Computer Vision 1(4):321–331.

[5] Berger, M.O. (1990). "Snake growing". In Faugeras, O., ed., Computer Vision – Proc. First European Conf. on Computer Vision (ECCV'90), Antibes, France, April, 1990, Lectures Notes in Computer Science, 570–572. Springer–Verlag.

[6] Cohen, L.D. (1991). On active contour models and balloons. CVGIP: Image Understanding 53(2):211–218.

[7] Ueda, N. and Mase, K. (1992). "Tracking moving contours using energy-minimizing elastic contour models". In Sandini, G., ed., Computer Vision – Proc. Second European Conf. on Computer Vision (ECCV'92), Santa Margherita Ligure, Italy, May, 1992, Lectures Notes in Computer Science, 453–457. Springer–Verlag.

[8] Rougon, N. and Prˆeteux, F. (1991). "Deformable markers: Mathematical morphology for active contour models control". In Image Algebra and Morphological Image Processing II, volume 1568 of SPIE Proc., 78–89. Bellingham, WA: SPIE.

[9] Cohen, L.D. and Cohen, I. (1993). "Finite element methods for active contour models and balloons for 2D and 3D images". IEEE Trans. on Pattern Analysis and Machine Intelligence 15(11):1131–1147.

[10] Leitner, F. and Cinquin, P. (1993). "From splines and snakes to Snakes Splines". In Laugier, C., ed., Geometric Reasoning: From Perception to Action, volume 708 of Lectures Notes in Computer Science. Springer–Verlag. 264–281.

[11] Carlbom, I., Terzopoulos, D. and Harris, K. (1994). "Computer-assisted registration, segmentation, and 3D reconstruction from images of neuronal tissue sections". IEEE Trans. on Medical Imaging 13(2):351–362.

[12] Gupta, A., O'Donnell, T. and Singh, A. (1994). "Segmentation and tracking of cine cardiac MR and CT images using a 3-D deformable model". In Proc. IEEE Conf. on Computers in Cardiology, September, 1994.

[13] Lobregt, S. and Viergever, M.A. (1995). "A discrete dynamic contour model". IEEE Trans. on MedicalImaging 14(1):12–24.

[14] Davatzikos, C.A. and Prince, J.L. (1995). "An active contour model for mapping the cortex". IEEE Trans. on Medical Imaging 14(1):65–80.

[15] Lin, W.C. and Chen, S.Y. (1989). "A new surface interpolation technique for reconstructing 3D objects from serial cross-sections". Computer Vision, Graphics, and Image Processing 48:124–143.

[16] Chang, L.W., Chen, H.W. and Ho, J.R. (1991). "Reconstruction of 3D medical images: A nonlinear interpolation technique for reconstruction of 3D medical images". Computer Vision, Graphics, and Image Processing 53(4):382–391.

[17] Terzopoulos, D. and Fleischer, K. (1988). "Deformable models". The Visual Computer 4(6):306–331.

[18] Amini, A.A., Weymouth, T.E. and Jain, R.C. (1990). "Using dynamic programming for solving variational problems in vision". IEEE Trans. on Pattern Analysis and Machine Intelligence 12(9):855–867.

[19] Poon, C. S., Braun, M., Fahrig, R., Ginige, A. and Dorrell, A. (1994). "Segmentation of medical images using an active contour model incorporating region-based images features". In Robb (1994), 90–97.

[20] McInerney, T. and Terzopoulos, D. (1995b). "Topologically adaptable snakes". In Proc. Fifth International Conf. on Computer Vision (ICCV'95), Cambridge, MA, June, 1995, 840–845. Los Alamitos, CA: IEEE Computer Society Press.

[21] Rougon, N. and Prˆeteux, F. (1991). "Deformable markers: Mathematical morphology for active contour models control". In Image Algebra and Morphological Image Processing II, volume 1568 of SPIE Proc., 78–89. Bellingham, WA: SPIE.

[22] Chakraborty, A., Staib, L.H. and Duncan, J.S. (1994). "Deformable boundary finding influenced by region homogeneity". In Proc. Conf. Computer Vision and Pattern Recognition (CVPR'94), Seattle, WA, June, 1994, 624–627. Los Alamitos, CA: IEEE Computer Society Press.

[23] Chakraborty, A. and Duncan, J.S. (1995). "Integration of boundary finding and region-based segmentation using game theory". In Bizais et al. (1995), 189–200.

[24] Herlin, I.L. and Ayache, N. (1992). "Features extraction and analysis methods for sequences of ultrasound images". Image and Vision Computing 10(10):673–682.

[25] Gauch, J.M., Pien, H.H. and Shah, J. (1994). "Hybrid boundary-based and region-based deformable models for biomedical image segmentation". In Mathematical Methods in Medical Imaging III, volume 2299 of SPIE Proc., 72–83. San Diego, CA: SPIE.

[26] Mangin, J.F., Tupin, F., Frouin, V., Bloch, I., Rougetet, R., Regis, J. and Lopez-Krahe, J. (1995). "Deformable topological models for segmentation of 3D medical images". In Bizais et al. (1995), 153–164.

[27] Vemuri, B.C. and Radisavljevic, A. (1994). "Multiresolution stochastic hybrid shape models with fractal priors". ACM Trans. on Graphics 13(2):177–207.

[28] Staib, L.H. and Duncan, J.S. (1992a). "Boundary finding with parametrically deformable models". IEEE Trans. on Pattern Analysis and Machine Intelligence 14(11):1061–1075.

[29] Worring, M., Smeulders, A.W.M., Staib, L.H. and Duncan, J.S. (1993). "Parameterized feasible boundaries in gradient vector fields. In Colchester", A.C.F. and

Hawkes, D.J., eds., "Information Processing in Medical Imaging". Proc. 13th Int. Conf. (IPMI'93), Flagstaff, AZ, June, 1993, Lectures Notes in Computer Science.Springer–Verlag. 48–61.

[30] Terzopoulos, D. and Fleischer, K. (1988). "Deformable models". The Visual Computer 4(6):306–331.

[31] T. McInerney and D. Terzopoulos (1995), "A dynamic finite element surface model for segmentation and tracking in multidimensional medical images with application to cardiac 4D image analysis," Comp. Med. Imag. Graph., vol. 19, no. 1, pp. 69–83.

[32] Malladi, R., Sethian, J.A., and Vemuri, B. (July 1993), "A Topology Independent Shape Modeling Scheme ", Proceedings of SPIE Conference on Geometric Methods in Computer Vision II, Vol. 2031, San Diego, California, pp. 246--258.

[33] Bakoš M. (Jan. 2007), "Active contour and their utilization at image segmentation", 5th Slovakian-Hungarian Joint symposium on applied machine intelligence and informatics, Poprad, Slovakia.

[34] Larie S. M. and Abukmeil S. S. (1998), "Brain abnormality in schizophrenia: a systematic and quantitative review of volumetric magnetic resonance imaging studies", J. Psych,. vol. 172, pp. 110–120.

[35] Taylor P. (1995), "Invited review: computer aids for decision-making in diagnostic radiology_a literature review", Brit. J. Radiol., vol. 68, pp. 945–957.

[36] Zijdenbos A. P. and Dawant B. M. (1994), "Brain segmentation and white matter lesion detection in MR images", Critical Reviews in Biomedical Engineering, vol. 22, pp. 401– 465.

[37] Worth A. J., Makris N., Caviness V. S., and Kennedy D. N. (1997), "Neuroanatomical segmentation in MRI: technological objectives", Int'l J. Patt. Recog. Artificial Intell., vol. 11, pp. 1161–1187.

[38] Davatzikos C. A. and Prince J. L. (1995), "An active contour model for mapping the cortex", IEEE Trans. Med. Imag., vol. 14, pp. 65–80.

[39] Khoo V. S., Dearnaley D. P., Finnigan D. J., Padhani A., Tanner S. F., and

Leach M. O. (1997), "Magnetic resonance imaging (MRI): considerations and applications in radiotheraphy treatment planning," Radiother. Oncol., vol.42, pp.1–15.

[40] Caselles V., Catte F., Coll T., and Dibos F. (1993), "A geometric model for active contours", Numerische Mathematik, vol. 66, pp. 1–31.

[41] Malladi R., Sethian J. A., and Vemuri B. C. (1995), "Shape modeling with front propagation: a level set approach", IEEE Trans. Pattern. Analysis. and Machine . Intelligence., vol. 17, no. 2, pp. 158– 175.

[42] Caselles V., Kimmel R., and Sapiro G. (1995), "Geodesic active contours", in Proc. 5th Int'l Conf. Comp. Vis., pp. 694–699.

[43] Whitaker R. T. (1994), "Volumetric deformable models: active blobs", Tech. Rep. ECRC-94- 25, European Computer-Industry Research Centre GmbH.

[44] Osher S. and Sethian J. A. (1998), "Fronts propagating with curvature-dependent speed: algorithms based on Hamilton-Jacobi formulations", J. Computational Physics, vol. 79, pp. 12–49.

[45] Sethian, J.A. (1982), "An Analysis of Flame Propagation", Ph.D. Dissertation, Dept. of Mathematics, University of California, Berkeley, CA.

[46] Sethian, J.A. (1985), "Curvature and the Evolution of Fronts", Comm. in Math. Phys., 101, pp. 487--499.

[47] Sethian, J.A. (1987), "Numerical Methods for Propagating Fronts in Variational Methods for Free Surface Interfaces", Proceedings of the Sept, 1985 Vallambrosa Conference, Eds. P. Concus and R. Finn, Springer-Verlag, NY.

[48] Sethian J.A.(1989), "A review of recent numerical algorithms for hyper surfaces moving with curvature dependent speed", J. Differential Geometry, vol. 31, pp. 131–161.

[49] Li C., Xu C. , Gui C. , and D. Fox M. (2005), "Level Set Evolution Without Re-initialization: A New Variational Formulation", proceedings of the 2005 IEEE Computer Society Conference on Computer vision and Pattern Recognition.

[50] Caselles V., Kimmel R., and Sapiro G.(1995), "Geodesic active contours", in Proc. 5th Int'l Conf. Comp. Vis., pp. 694–699.

[51] Caselles V., Kimmel R., and Sapiro G.(1997), "Geodesic active contours", Int'l J. Comp. Vis., vol. 22, pp. 61–79.

[52] Yezzi A., Kichenassamy S., Kumar A., Olver P., and Tennenbaum A. (1997), "A geometric snake model for segmentation of medical imagery", IEEE Trans. Med. Imag., vol. 16, pp. 199–209, 1997.

[53] Kichenassamy S., Kumar A., Olver, A. Tennenbaum P., and Yezzi A. (1996) "Conformal curvature flows: from phase transitions to active vision", Arch. Rational Mech. Anal., vol. 134, pp. 275–301.

[54] Siddiqi K., Lauzi`ere Y. B., Tannenbaum A., and Zucker S. W.(1998), "Area and length minimizing flows for shape segmentation", IEEE Trans. Imag. Proc., vol. 7, pp. 433– 443.

[55] Zhang H., Morrow P, McClean S, and Saetzler K. (2008), "Contour Detection of Labelled Cellular Structures from Serial Ultrathin Electron Microscopy Sections using GAC and Prior Analysis", Image Processing Theory, Tools & Applications.

[56] Cohen L.D.(1991), "On active contour models and balloons", Computer Vision, Graphics and Image Processing: Image Understanding, 53(2): 211-218.

[57] MacQueen, J. B. (1967). "Some Methods of Classification and Analysis of Multivariate Observations". Proceedings of 5th Berkeley Symposium on Mathematical Statistics and Probability. **1**: 281–297, University of California Press. MR0214227. Zbl 0214.46201. Retrieved on 2009-04-07.

[58] Osher S. and Paragios N. (2003), "Geometric Level Set Methods in Imaging Vision and Graphics", Springer Verlag, ISBN 0387954880.

[59] Shi J. and Malik J. (1997): "Normalized Cuts and Image Segmentation", IEEE Conference on Computer Vision and Pattern Recognition, pp 731-737.

[60] Beucher S. and Meyer F. (1993), "The morphological approach to segmentation: the watershed transformation". Mathematical Morphology in Image Processing (Ed. E.R. Dougherty), pages 433-481.

[61] Lindeberg T. (1993), "Detecting salient blob-like image structures and their scales with a scale-space primal sketch: A method for focus-of-attention". International Journal of Computer Vision, 11(3), 283--318.

[62] Ultsch, Alfred (2007). "Emergence in Self-Organizing Feature Maps". In Proceedings Workshop on Self-Organizing Maps (WSOM '07). Bielefeld, Germany. ISBN 978-3-00-022473-7.

[63] http://math.berkeley.edu/~sethian/2006/Applications/Medical_Imaging/artery.html, Copyright:1996,1999,2006 J.A. Sethian.

[64] Bakoš M., (2007), "Active Contours and their Utilization at Image Segmentation". 5th Slovakian-Hungarian Symposium on Applied Machine Intelligence and Informatics. Popard, Slovakia.

[65] Xu C., Pham D. L., and Prince J. L.,(2000), "Medical Image Segmentation Using Deformable Models". SPIE Handbook on Medical Imaging -- Volume III: Medical Image Analysis, edited by J.M. Fitzpatrick and M. Sonka.

[66] Gonzalez R. C., and Woods R. E., (2008), "Digital Image Processing", third edition, Pearson Prentice Hall, 264-266.

[67] Graps A. (1995), "An Introduction to Wavelets", IEE Computational Science and Engineering, vol.2.

[68] Tang J., (2009), "A multi-direction GVF snake for the segmentation of skin cancer images", Pattern Recognition, 42 1172 – 1179.

[69] Kachouie N. N., Fieguth P, and Rahnamayan S., (2006), "An Elliptical Level Set Method for Automatic TRUS Prostate Image Segmentation", IEEE International Symposium on Signal Processing and Information Technology.

[70] Xianfen D., Siping C., Changhong L., Yuanmei W., (2005), "3D Semi-automatic Segmentation of the Cochlea and Inner Ear", Proceedings of the 2005 IEEE Engineering in Medicine and Biology 27th Annual Conference Shanghai, China, September 1-4.

 [71] *Bodkhe S. T.*, *Raut S. A.,(2008), "*A Unique Method for 3D MRI Segmentation", International Conference on Computer Science and Information Technology.

[72] Chena Y.-C., Chena Y.-C., (2008), "Ann-Shyn Chiang Template-driven segmentation of confocal microscopy images", computer methods and programs in biomedicine 89, 239–247.

[73] Pang B., Zhang D., and Wang K.*,* (2005), "The Bi-Elliptical Deformable Contour and Its Application to Automated Tongue Segmentation in Chinese Medicine", IEEE transactions on medical imaging, vol. 24, no. 8, august 2005.

[74] Makowski P., Sφrensen T. S., Therkildsen S. V.,Materka A.,Jorjensen H. S., and Pederson E. M.,(2002), "Two Phase Active Contour Method for Semiautomatic

Segmentation of Heart and Blood Vessels from MRI Images for 3D Visualization", Computer Medical Imaging and Graphics 26, 9-17.

[75] Zouridakis G., Doshi M., and Mullani N.,(2004) ,"Early Diagnosis of Skin Cancer Based on Segmentation and Measurement of Vascularization and Pigmentation in Nevoscope Images", Proceedings of the 26th Annual International Conference of the IEEE EMBS San Francisco, CA, USA, September 1-5-2004.

[76] Kim J., Cai W., Eberl S., and Feng D., (2007), "Real-Time Volume Rendering Visualization of Dual-Modality PET/CT Images With Interactive Fuzzy Thresholding Segmentation", IEEE Transactions on Information Technology in Biomedicine, vol. 11, no. 2, march 2007.

[77] Bhanu B., and Peng J., "Adaptive Integrated Image Segmentation and Object Recognition",(2000), IEEE Transactions on Systems, Man, and Cybernetics—Part c: Applications and Reviews, vol. 30, no. 4, November 2000.

[78] Saito Y., Kenmochi Y., and Kotani K., "Extraction of A Symmetric Object for Eyeglass Face Analysis Using Active Contour Model", 0-7803-6297-7/00/ ©2000 IEEE.

[79] Boykov Y., Funka-Lea G., (2006), "Graph Cuts and Efficient N-D Image Segmentation". International Journal of Computer Vision 70(2), 109–131.

[80] Amonou I., Duhamel P., "Iterative Backward Segmentation for Hierarchical Wavelet Image Coding", 0-7803-6297-7/00 © 2000 IEEE.

[81] Tsai T.-H., Chen G.-J., and Tzeng W.-L., "A Novel Foreground/Background Decision using in Unsupervised Segmentation of Moving Objects in Video Sequences", 0-7803-8294-3/04 ©2004 IEEE 1587.

[82] Liu Y., Peng S., (2008), "A New Motion Detection Algorithm Based on Snake and Mean Shift". Congress on Image and Signal Processing.

[83] Kim M., Choi J. G., Kim D., Lee H., Lee M. H., Ahn C., and Ho Y.-S., (1999), " A VOP Generation Tool: Automatic Segmentation of Moving Objects in Image Sequences Based on Spatio-Temporal Information", IEEE Transactions on Circuits and Systems for Video Technology, vol. 9, no. 8.

[84] Cai H., Xu X., Lu J., Lichtman J. W., Yung S.P., and Wongc S. T.C., (2006) "Repulsive force based snake model to segment and track neuronal axons in 3D microscopy image stacks", NeuroImage, 32, 1608 – 1620.

[85] Moghaddam M. K., Safabakhsh R., "TASOM-Based Lip Tracking Using the Color and Geometry of the Face", Proceedings of the Fourth International Conference on Machine Learning and Applications (ICMLA'05)

[86] Ng H.P., Ong S.H., Foong K.W.C., Goh P.S., Nowinski W.L. "Medical Image Segmentation Using K-Means Clustering and Improved Watershed Algorithm", 1-4244-0069-4/062006 IEEE.

[87] Rezaee M. R., van der Zwet Pieter M. J., Lelieveldt B. P. F., van der Geest, and Reiber J. H. C.,(2000) "A Multiresolution Image Segmentation Technique Based on

Pyramidal segmentation and fuzzy clustering". IEEE Transactions on Image Processing, vol. 9, no. 7.

[88] Xue H., Gdraudi, A, and. Duvet-Lutz, "Multi-Band Segmentation Using Morphological Clustering and Fusion - Application to Color Image Segmentation", 0-7803-7750-8 © 2003 IEEE.

[89] Wang W., Zhao X., and Feng X., "Parallel Wavelet-Based Image Segmentation Using MPI ", 0-7803-8560-8/04 ©2004 IEEE

[90] Yang G., Chen K., Zhou M., Xu and Z., Chen Y., "Study on Statistics Iterative Thresholding Segmentation Based on Aviation Image". Eighth ACIS International Conference on Software Engineering, Artificial Intelligence, Networking, and Parallel/Distributed Computing.

[91] Wang W., "Colony Delineation on Image Classification". The 18th International Conference on Pattern Recognition (ICPR'06).

[92] Sofou A. and Maragos P., "Generalized Flooding and Multicue PDE-Based Image Segmentation", IEEE Transactions on Image Processing, Vol. 17, No. 3, March 2008.

[93] Deng Y., and Manjunath B.S., "Unsupervised Segmentation of Color-Texture Regions in Images and Video". IEEE Transactions on Pattern Analysis and Machine Intelligence, Vol. 23, No. 8, August 2001.

[94] Ji L., (2002), "Hong Yan Attractable snakes based on the greedy algorithm for contour extraction". Pattern Recognition 35 , 791–806.

[95] Brej M., and Sonka M., (2000), "Object Localization and Border Detection Criteria Design in Edge-Based Image Segmentation: Automated Learning from Examples". IEEE Transactions on Medical Imaging, Vol. 19, No. 10.

[96] Wang W. and Stephansson O., "A Robust Bubble Delineation Algorithm for Froth Images", 0-7803-5489-3/99 ©1999 IEEE.

[97] Katsoulas D., Bastidas C. C., and Kosmopoulos D.,(2008), "Super-quadric Segmentation in Range Images via Fusion of Region and Boundary Information". IEEE Transactions on Pattern Analysis and Machine Intelligence, Vol. 30, No. 5.

[98] Wang S., and Siskind J. M., (2003), "Image Segmentation with Ratio Cut". IEEE Transactions on Pattern Analysis and Machine Intelligence, Vol. 25, No. 6.

 [99] Lin Y.-C., Tsai Y.-P., Hung Y.-P., and Shih Z.C., (2006), "Comparison Between Immersion-Based and Toboggan-Based Watershed Image Segmentation". IEEE Transactions On Image Processing, Vol. 15, No. 3.

[100] Ng H.P., Ongc S.H., Foonga K.W.C., Goh P.S., Nowinskib W.L., (2008), "Masseter Segmentation Using An Improved watershed Algorithm With Unsupervised Classification". Computers in Biology and Medicine 38 171 – 184.

[101] Ding J., Ma R., and Chen S., (2008), "A Scale-Based Connected Coherence Tree Algorithm For Image Segmentation". IEEE Transactions On Image Processing, Vol. 17, No. 2.

[102] Färber M., Ehrhardt J., Handels H., (2007) "Live-Wire-Based Segmentation Using Similarities Between Corresponding Image Structures". Computerized Medical Imaging and Graphics 31, 549–560.

[103] Zhao H.K., Chan T., Merriman B. and Osher S.J., (1996), ``A Variational Level Set Approach to Multi-Phase Motion", *J. Comp. Phys*., **115**, 179-195.

[104] http://fas.sfu.ca/, Blair Mackiewich, Sat Aug 19 16:59:04 PDT 1995

VITAE

Name: Sharif Mohammad Saleh Al-Sharif.

Place of Birth: Hebron – Palestine.

Date of Birth: 1st Aug. 1978.

Nationality: Palestinian.

Education: Jan. 2010: M.Sc. in Systems Engineering, King Fahd University of

Petroleum & Minerals, Dhahran – Saudi Arabia.

Dec. 2005: Diploma in "Training of Trainers", Palestine

Polytechnic University, Hebron – Palestine.

Feb. 2002: B.Sc. in Electrical Engineering, Palestine Polytechnic

University, Hebron – Palestine.

Mailing Address: Dammam Korniche, Dammam, Saudi Arabia.

Tel. +966 (0)56 955 14 48.

Permanent Address: University Quarter, Hebron, Palestine.

Tel: +970 (0)2 2228565.

Email: sharif182@yahoo.co.uk.